Overview on the strong motion data recorded during the May-June 2012 Emilia seismic sequence

Lucia Luzi [1] Francesca Pacor [1], Gabriele Ameri [1], Rodolfo Puglia[1], Pierfrancesco Burrato[2], Marco Massa [1], Paolo Augliera[1], Gianlorenzo Franceschina[1], Sara Lovati[1] and Raul Castro[3].

[1] Istituto Nazionale di Geofisica e Vulcanologia, via Bassini 15, 20133 Milano, Italy.

[2] Istituto Nazionale di Geofisica e Vulcanologia, via Vigna Murata 608, 00143 Roma, Italy.

[3] Departamento de Sismología, División Ciencias de la Tierra, centro de Investigación Científica y de Educación Superior de Ensenada (CICESE), Ensenada, Baja California, 22860, México.

Corresponding author:

Lucia Luzi,

Istituto Nazionale di Geofisica e Vulcanologia

via Bassini 15, 20133 Milano, Italy

e-mail: lucia.luzi@mi.ingv.it

1. INTRODUCTION

On 20 May 2012, at 02:03:52 GMT, an earthquake with Mw 6.1 (RCMT, http://www.bo.ingv.it/RCMT) occurred in northern Italy striking a densely populated area. The mainshock was followed a few hours later by two severe aftershocks having the same local magnitude (Ml 5.1, 1 and 2 in Figure 1a), and by hundreds of smaller aftershocks. Nine days later, on 29 May, at 07:00:03 GMT, a second event with moment magnitude Mw 6.0 (RCMT, http://www.bo.ingv.it/RCMT) occurred to the west, on an adjacent fault segment. This event was also followed by hundreds of aftershocks, three of them having local magnitude 5.3, 5.2 and 5.1 (3, 4 and 5, respectively, in Figure 1a) (locations from Istituto Nazionale di Geofisica e Vulcanologia, hereinafter INGV, http://iside.rm.ingv.it/; Malagnini et al., 2012; Scognamiglio et al., 2012). Despite the moderate number of casualties if compared to other major events in the Italian history, the economic loss was extremely high, resulting in about EUR 5 billion (AON Benfield, 2012, http://www.aon.com/), as the majority of Italian industrial activities and infrastructures concentrate in this area, the eastern Po plain, which is the largest sedimentary basin in Italy.

The mainshocks are associated to two thrust faults with an approximate E-W trend dipping to the South (Figure 1b). The majority of the faults in this region are located in the upper crust, at depths lower than 10 km. The two main shocks are among the strongest earthquakes generated by thrust faults ever recorded in Italy in the instrumental era. The Emilia sequence has been extensively recorded by several strong-motion networks, operating in the Italian territory and neighbouring countries. Some of the networks acquire continuous data streams at their national data centres, which are nodes of EIDA (European Integrated Data Archive, hhtp://eida.rm.ingv.it), a federation of several archives, so that the waveforms can be obtained immediately after the occurrence of an event. Other networks, such as the Italian accelerometric network (RAN), managed by the Italian Department of the Civil Protection (hereinafter DPC), distribute the acceleration waveforms through their web site (http://protezionecivile.gov.it).

The data set explored in this study is relative to the six events of the sequence having Ml > 5 (Table 1) and consists in 365 accelerograms recorded within a distance of 200 km from the epicentres, that were provided by the permanent and temporary seismic networks of INGV, the Swiss Seismological Service (SED, http://www.seismo.ethz.ch/index) and the DPC. This data set has no equals in Italy, as, for the first time after the 1976 Friuli, sequence (Mw 6.4 on 1976-05-06; Mw 5.6 on 1976-09-11; Mw 5.9 on 1976-09-15 at 03:15:18 and Mw 6.0 1976-09-15 at 09:21:18, all magnitudes provided by Pondrelli et al. 2001) major earthquakes have been recorded in the Po plain. The geologic features of northern Italy are also unique, as the Po plain is one of the largest sedimentary basins in the world with an area of about 50.000 km^2 and a sediment thickness varying from few tens of meters to about 8 km. In general, most of the urban regions are situated on deep sediment-filled basins where large amplitude ground motions have been observed at long periods. Besides the amplification due to the soft surface layers, the basin structure may also trap the incoming seismic waves and convert the body waves into surface waves, thus prolonging the ground shaking within the basin. These phenomena have been observed, or simulated for different structures, such as the Los Angeles basin (Hanks, 1975; Joyner, 2000; Somerville et al., 2004), for which a data set was recently compiled by Steidl and Lee (2000), the Osaka Basin in Japan (Kagawa et al., 2004) and the Kanto basin beneath the city of Tokyo (Hisada et al., 1993; Sato et al. 1999).

This paper provides an overview of the strong motion data for the six events having M > 5, highlighting the key features of strong motion observations in terms of spectral content, peak amplitudes and attenuation of spectral ordinates as function of distance from the source and geologic conditions.

In particular, our study will focus on: i) observations on the strong motion signals; ii) spatial distribution of ground motion at regional scale (northern Italy) and correlation with the geologic structure of the southern Alps and the northern Apennines; iii) fit of the Emilia strong motion dataset with a set of ground motion prediction equations developed for Italy (ITA10, Bindi et al.,

2011), including a residual analysis. The last point is particularly worth of interest since ITA10 model was calibrated on a data set consisting almost entirely of crustal events recorded in the central – southern Apennines, where the geologic conditions are totally different from those of Northern Italy.

2. GEOLOGIC OVERVIEW AND HISTORICAL SEISMICITY

The Po plain is the foreland basin of two opposing verging fold-and-thrust belts: to the north, the south-verging central Southern Alps (hereinafter SA), which is the conjugate retro-belt with respect to the subduction polarity of the Alpine orogen, and, to the south, the N-NE-verging Northern Apennines (hereinafter NA). The two belts developed during the closure of the Mesozoic Tethyan basin occurring in the framework of the African and European plates relative convergence from the Cretaceous onward, and were associated with two opposite subduction zones involving both European and African lithosphere (for an in-depth review see Carminati and Doglioni, 2012, and reference therein).

The morphological borders of the plain defined by the two mountain chains corresponds also to the contact between the Quaternary alluvium, outcropping in the plain, and the pre-Quaternary rocks exposed along the mountain fronts (Figure 1a). Albeit its almost flat morphology, due to active fluvial deposition, the Po plain is far to be an undeformed domain, since the outermost and most recent thrust fronts of the two belts are buried by the Plio-Quaternary sedimentary sequence. This is reflected by a variable sediment thickness, ranging between several thousands of meters in the depocenters and few tens of meters on top of the buried anticlines (Bigi et al., 1992). The thickness of the sedimentary wedge generally increases towards the NA mountain front and the basal detachment of the thrust wedge becomes deeper in the same direction (Figure 1b).

The outermost thrust fronts of the NA belt, buried below the Plio-Quaternary marine and continental deposits infilling the Po plain basin, are organized in three complex systems of folds:

the Monferrato, the Emilian, and the Ferrara arcs, from west to east. The shallow and deep subsurface geology of the Po plain was constrained by a great amount of data gathered in the framework of hydrocarbon exploration (e.g. Fantoni and Franciosi, 2010), hydrogeological studies (R.E.R. and ENI-AGIP, 1998) and the new Geological Map of Italy (1:50,000 scale; available from http://sgi.isprambiente.it/geoportal). These subsurface data show a system of N to NE-verging blind thrusts and folds that controlled the deposition of the syntectonic sedimentary wedges. Fast sedimentation (Bartolini et al., 1996) concealed the growing structures, and, as a consequence, today there is limited direct evidence of the possible ongoing activity of the thrusts. One of the few and most notable exceptions to this general rule is the San Colombano Hill, an emerging anticline located at the leading edge of the Emilian Arc, involving upper Pliocene and lower Pleistocene sediments and cored by Miocene deposits. In its turn, the buried outer thrust front of the central SA mainly developed during Oligocene to Late Miocene with a simpler geometry describing a single wide arc between Milano and the Garda Lake. This arc is connected to the east with the NNE-trending Giudicarie thrust system, considered a regional transfer zone between the Central and Eastern Southern Alps (e.g. Castellarin and Cantelli, 2000). The S-verging frontal thrust system is characterized by the occurrence of high angle back-thrusts associated with some small outcropping anticlines first investigated by Desio (1965) (see also Livio et al., 2009).

As a whole the Quaternary stratigraphy records a regressive sequence, having at the base a thick layer of marine deposits (early Pliocene to early Pleistocene, Capozzi and Picotti, 2003), followed by shallow marine and littoral deposits interfingered with alluvial plain sediments (0.9 My, e.g. Amorosi et al., 1998), further followed by fully continental alluvial deposits of the Emiliano-Romagnolo Inferiore Synthem (AEI, 0.75 My), and of the Emiliano-Romagnolo Superiore Synthem (AES, 0.45/0.35 My).

Crustal deformation analysis of GPS data constrains limited shortening in the Po plain across the NA and SA fronts with rates around 1 mm/a (e.g. Devoti et al., 2011). Present-day activity of the frontal thrusts of the NA and SA belts is also testified by historical and instrumental seismicity, the

latter characterized by compressive focal mechanisms (e.g. Pondrelli et al., 2006; see also the focal solutions of the 2012 Emilia sequence in Pondrelli et al., 2012 and Scognamiglio et al., 2012), and by the influence of faulting and folding of recent sediments on the drainage network (Burrato et al., 2003; Burrato et al., 2012). The historical and instrumental Italian seismic catalogues show that the southern Po plain is affected by low to moderate seismicity, with Mw up to 5.8 (Castello et al., 2006; DISS Working Group, 2010; CPTI11 Catalogue, Rovida et al., 2011). Borehole breakouts and focal mechanisms all show maximum shear stress oriented perpendicular to the trend of the buried thrust fronts in agreement with geological and seismological evidence of active compression (Montone et al., 2012).

3. STRONG MOTION DATA SET

The data set used in this study consists of waveforms recorded by the accelerometers of the Italian Department of the Civil Protection, the Istituto Nazionale di Geofisica e Vulcanologia and the Swiss Seismological Service. This data set, resulting from earthquakes occurring on a system of thrust faults, is of major relevance, as the Italian strong motion catalogue is mainly composed of records from earthquakes with normal focal mechanism recorded in the central-southern Apennines. Figure 2 shows the magnitude histogram and the distance versus magnitude distribution of the 365 strong motion records from the 6 earthquakes examined (Table 1) and the 153 stations examined (Figure 3 and Table 2). Comparing with the entire Italian data set for reverse fault, used to derive Italian GMPEs (Bindi et al., 2011), the records from reverse fault mechanism represented only about 10% of the totality of strong-motion records in Italy (Pacor et al., 2011).

In Table 2 the characteristics of the recording stations within a distance of 200 km from the epicentre are described. They are classified as in the Italian Accelerometric Archive (ITACA), according to the average shear wave velocity of the uppermost 30 m, $V_{S,30}$ (Comité Européen de Normalisation, 2004) where the velocity of class A is larger than 800 m/s, B is in the range 360–

800 m/s, C in the range 180–360 m/s, and D is less than 180 m/s. The classes not denoted with an asterisk have been assigned after a direct measure of $V_{S,30}$, the ones with an asterisk have been attributed on the basis of geological/geophysical information (Pacor et al., 2011; Di Capua et al., 2011), and, as first approximation, the new stations, not included in the ITACA database, and located in the Po plain, were assigned to class C and denoted with a double asterisk.

The strong motion stations are equipped with Kinemetrics Episensor or Syscom MS2007+, which are triaxial force balance sensors, with a natural frequency above 50 Hz set to 1 or 2 g fullscale. They are coupled with different digitizers (Reftek 130-01, Kinemetrics Etna Everest or K2, Quanterra Q330, or GAIA2, Geophisical All Inclusive Aquisitor, of INGV design and manifacture, Salvaterra et al., 2008) with resolution higher than 22 bits and 100 or 200 Hz sampling. The recorded waveforms are processed adopting the procedure described in Pacor et al. (2011) and Paolucci et al. (2011). This method includes the removal of the linear trend fitting the entire record, a cosine taper, and the application of a time-domain acausal 4th-order Butterworth band-pass filter. Before executing the filtering procedure zero pads are added, as in Boore and Bommer (2005), in order to reduce the sampling interval in the frequency domain and thus increase the accuracy in the low frequency filtering. Both the high-pass and low-pass frequencies are selected through visual inspection of the Fourier spectrum. The typical band-pass frequency range is between 0.08 and 40 Hz. Zero pads are then removed from the filtered signal and a procedure is applied in order to guarantee the compatibility between acceleration velocity and displacement by subsequent integration.

The event of the 20 May 2012 (Mw 6.1, RCMT, http://www.bo.ingv.it/RCMT) has been recorded by 179 digital stations, 126 of which within a distance of 200 km from the epicentre. The epicentral distances range from 13 km to about 550 km. Twenty stations have Joyner-Boore distances (hereinafter R_{JB}) ranging from about 1 to 60 km, but only one site, Mirandola (MRN), is located at 1.3km from the fault, while the others are at distances larger than 20km (Figure 3). The highest recorded PGAs and PGVs are 259 cm/sec^2 and 46 cm/s, respectively, for the horizontal

components, and 297 cm/sec^2 and 6 cm/s for the vertical, all of them recorded at MRN station. The rest of the observed PGAs and PGVs do not exceed 50 cm/sec^2 and 7cm/s, respectively.

The event of 29 May 2012 (Mw 6.0, RCMT, http://www.bo.ingv.it/RCMT) was recorded by 120 stations within an epicentral distance of 200 km. Several temporary stations were installed after the shock of May 20th, including 8 by RAN (www.protezionecivile.gov.it) and 7 by INGV (www.ingv.it), in order to increase the network density (ten stations are within a R_{JB} distances of 20 km). The horizontal PGAs are lower than 300 cm/sec^2 with the largest values observed at MRN (280 cm/ sec^2) and CNT (294 cm/ sec^2), located respectively at R_{JB} = 0 and R_{JB} = 19 km. Very high PGA values were recorded on the vertical component at MRN, reaching 840 cm/sec^2.

4. WAVEFORMS FEATURES

The waveforms recorded during the main events of the Emilia sequence are rather uncommon compared to the Italian strong motion recordings, due to the relevant, and in many cases dominant, presence of surface waves (Love and Rayleigh waves). Near-source records are particularly complex, because of the superposition of body and surface waves with the latter having the largest amplitudes. This is unexpected in near-source condition where S waves usually have the prevalent contribution.

In Figure 4 we present two records of the 29 May event, which exemplify the characteristics of the Emilia seismic signals. Figure 4a shows the time series (acceleration, top, and velocity, bottom, of the vertical and the NS components) of a temporary station, MOG0, located at 19km from the hypocenter, where surface waves are observed contemporary to S waves. Figure 4b shows the records of the station Oppeano (OPPE), located at 51 km from the hypocentre, where surface waves are evident after a lag of about 15s with respect to the S waves arrival and cause an increase of the significant duration of the signal. The PGVs are always observed within the surface wave phase, whereas the PGAs can be either associated to the S or the surface waves, at distances lower than

about 80 km, and to the S-phase at epicentral distances larger than 100 km. These features are valid for both the vertical and the horizontal components.

As a consequence of later surface wave arrivals, the duration of the significant part of the signal (measured as the time between the release of 5% and 95% of the total Arias Intensity) can be extremely variable, being very short in the vicinity of the source and as large as 100 – 120s at epicentral distances larger than 30 km and, in general, directly proportional to the distance from the epicentre. This effect is exemplified in Figure 5, where the stations MRN and the MODE are shown.

The surface waves do not show an isotropic propagation pattern throughout the Po plain. This phenomenon can be evidenced by the time-frequency analysis of the recordings, applying the S-transform method (Stockwell et al. 1996), which allows identifying the arrival times and frequencies of different phases in a seismic signal. In Figure 6, the total power spectrum (Pinnegar, 2006) of the velocity time series relative to the event of May 20 are plotted for significant stations located at different azimuths and distances from the epicentre. In general, the surface waves are mostly evident in the records of the stations located from NNE to SSW where the largest total power spectrum can be observed at frequencies below 0.5 Hz.

In detail, NNE with respect to the epicentre, a clear presence of surface waves, with frequency of 0.2 and 0.5 Hz, is observed at stations OPPE and ISD, both at distance of about 50 km, starting at about 20s after the P-phase arrival. These phases carry the largest energy and the peak ground velocity. At distances larger than 100 km (stations CRND, ASOL) a dominant, a 0.2 Hz quasi monochromatic surface wave arrival can be observed at about 50s after the P-phase with amplitude comparable to the one of the S phase. The OPPE and ISD stations are located on an almost undeformed part of the northern Po plain foreland, where the depth of the base of the Plio-Quaternary sediments thickens southward following the regional monocline (e.g. Mariotti and Doglioni, 2000). Conversely, the CRND and ASOL stations are installed on the small hills at the northern margin of the Venetian plain made of pre-Quaternary bedrock outcrops. Surface waves

with frequency in the range 0.2 – 0.5 Hz are also evident east of the epicentre (station ARG, R = 55km), and to the south (stations ZPP and MDN, R = 40 km). The ARG station is located on a shallow buried fold of the outer NA thrust front, whereas the ZPP and MDN on relatively deep thrust-top basins close to the mountain front where the thickness of the Plio-Quaternary sediments is highly variable. At distances of about 150 km to the south, stations FIR and OSSC, also recorded the quasi monochromatic 0.2 Hz surface wave observed at CRND and ASOL, which does not attenuate through the Apennines.

An additional observation regards the frequency content of the signals: records at distances less than 60 km from the epicentre have a broadband frequency content, while, at increasing distances, there is a persistent frequency of about 0.2 Hz, which is probably the frequency at which the eastern Po plain vibrates. On the contrary, to the west (station SRP), surface waves carry very low energy, as shown by the amplitudes of the total power spectrum, and there is almost no evidence of the 0.2 Hz surface wave, which probably attenuates through the western sediments which differ in thickness, composition and age from the eastern Po plain (Figures 1b and 3). In particular the SRP station locates on the deeper part of the undeformed Po plain foredeep basin, just outside of the Ferrara arc. Similar observations can be drawn for the records of May 29, although the 0.2 Hz surface waves attenuate faster travelling throughout the Apennines, therefore the total power spectra have lower amplitudes than the ones calculated for the records of May 20.

5. SPATIAL VARIABILITY OF GROUND-MOTIONS RECORDED DURING THE MAJOR EVENTS OF THE EMILIA SEQUENCE

In order to give a global overview of the spatial variability of the ground motion recorded during the major events of the Emilia sequence, peak values and spectral ordinates observed at single sites have been interpolated via the kriging algorithm (Davis 1973), which predicts unknown values using variograms to express the spatial variation and minimizes the error of predicted values. In

particular, a spherical semivariogram model with nugget is adopted. The software used to perform the kriging analyses is mGstat (mgstat.sf.net), which runs under MatLab®.

Shakemaps relative to the May 20 and 29 events, calculated from a similar station set, are published (e.g. http://shakemap.rm.ingv.it/shake/ 8222913232/pga.html and http://shakemap.rm.ingv.it/shake/7223045800/pga.html for PGA, but also available for PGV, PSA at 0.3s 1.0s and 3.0s). Shakemaps aim at a picture of ground shaking, with particular emphasis in the epicentral area, using both observations and predictions from a GMPE, while the maps produced in this study are exclusively based on observations and aim at defining the attenuation trend over a larger area (e.g. northern Italy). In general, the agreement between the two products is good, although minor differences can be attributed either to the interpolation algorithm or the input data (e.g. different stations or peak parameters obtained from different processing procedures applied to the accelerometric or velocimetric time series). The larger differences are evident for the May 20 event, as at that time the station density was poor in the epicentral area, and the ground shaking obtained by the shakemaps is mainly controlled by the GMPE values.

Figure 7 shows the spatial distribution of the geometrical mean of the two horizontal components for the Peak Ground Acceleration (PGA), Peak Ground Velocity (PGV) and Peak Ground Displacement (PGD) of the two main events.

The general trend of PGA is a slow decay rate towards north (at stations MNS or ZOVE, Figure 3), where the rock formations of SA crop out, or where the sediments of the Po plain are thinner (at stations SANR, OPPE, Figure 3), and a strong attenuation to the S and to the SW, in correspondence of western NA. This evidence is also found by Morasca et al. (2010), who attribute it to the high heat flow in the lower crust beneath Tuscany.

Although the interpolation is not well constrained to the E due to the poor station coverage, the PGV and PGD values of the event of 20 May are much larger to the east than to the west (stations ARG and FAEN, Figure 3), while the same trend is not clearly visible for PGA.

The area enclosing the largest peak values at low frequencies (PGD > 3 cm) is smaller on May 29 than on May 20, although the two magnitudes are very similar. This suggests that low frequency source effects could have affected the ground motion of the May 20 recordings.

PGV and PGD, as stated before, generally occur within surface waves arrival, therefore, as observed in the analysis of the single signals (Figure 6), they sharply attenuate to the west and south-west, while the largest amplitudes are observed at the eastern Po plain. The PGV and PGD pattern seems to be correlated to the structure of the Ferrara arc, since most of the largest amplitudes registered in this part of the Po plain are confined between the outer NA thrust front and the mountain front. Relatively large amplitudes, although lower than those recorded in the Ferrara arc, are also found in the Venetian plain. The pattern of low-frequency wave phases is striking when interpolating the displacement spectra (5% damping) ordinates at periods of 1s, 4s and 10s, for the geometric mean of the two horizontal components (Figure 8). While the 1s displacement spectrum ordinates reflect the trend of PGV, the spectral ordinates at long periods define almost exactly the limits of the sediments of the Po plain, especially for the main event, indicating that the entire Po plain can be affected by large amplitude long period ground motion in case of a moderate to large event.

In the following sections the observed ground motion values will be compared to the predictions of a set of equations developed for the Italian territory (Bindi et al., 2011) and for Northern Italy (Massa et al., 2008), in order to evaluate the importance and the peculiarities of the energy content released at low frequencies for this region.

6. RESIDUAL ANALYSIS WITH RESPECT TO A SET OF GROUND MOTION PREDICTION EQUATIONS DEVELOPED FOR ITALY

PGA, PGV and acceleration spectral ordinates (5% damping) recorded during the six events (M > 5) listed in Table 1 are compared with two ground motion prediction equations (GMPEs): i) Bindi et al. (2011), hereinafter referred to as ITA10, valid for the Italian territory, recently derived from a

qualified data set almost entirely consisting of crustal events recorded in the central – southern Apennines; ii) Massa et al. (2008), hereinafter MS08, calibrated with a data set of waveforms recorded in northern Italy.

ITA10 accounts for a linear and a quadratic magnitude term, a magnitude dependent geometrical spreading, an anelastic attenuation term, style of faulting coefficients and 5 soil types, as in the Eurocode 8 (EC8) classification. MS08 adopts a simpler functional form and contains only the linear term for magnitude, a geometrical spreading independent on magnitude, no style of faulting and 2 soil classes (rock / soil). In Figure 9 and 10 the observations of the Emilia earthquake are compared to ITA10 for a visual comparison, with the aim of detecting differences between the ground motion parameters recorded in Northern Italy and the mean parameters predicted for the Italian territory.

Figure 9 shows the PGA and PGV and the spectral ordinates at two periods (T = 2s and T = 4s) estimated by the ITA10 model compared with the observed ones for the 20 May earthquake. Reverse fault mechanism and appropriate site conditions are assumed. Due to the poor information on the local site conditions, the observations were grouped into two classes: soft sites (EC8 class C, white circles, for a comparison with ITA10 class C) and rock and stiff soil (EC8 class A and B, gray circles, for a comparison with ITA10 class A). The comparison of the geometric mean of the horizontal components up to 200 km (Figures 9a - 9b) indicates that, in general, the agreement between observations and predictions is good with few exceptions. In particular, the observed PGAs and PGVs decay faster than ITA10 at distances larger than 40 km, as the majority of observations fall below the median minus one standard deviation. At distances less than 10 km, the observed PGA at station MRN is within the mean minus one standard deviation, while the opposite in observed for PGV, as the value recorded at MRN is within one standard deviation above the mean. Figures 9c and 9d show the vertical PGAs and PGVs compared to the ITA10: the observed PGAs for EC8 C sites are lower than the mean predictions at distances larger than 20 km. In terms of vertical PGV, the ITA10 predictions for EC8 C sites overestimate the observed peak values that

decay with distance similarly to the mean for EC8 A sites. This feature suggests a significant attenuation of the high-frequency wavefield in the Po plain sediments. To highlight the low frequency characteristic of the Emilia earthquake ground motion, in Figure 9e and 9f we compare the decay of observed acceleration spectral ordinates (at 5% damping) of the horizontal components at 2s and 4s, with the ITA10, whose coefficients have been evaluated up to 4s, although they have been published up to 2s.

For the majority of EC8 C sites within 100 km from the source, the discrepancy between median predictions and observations increases at increasing period. At T = 2s, the observations fit the predictions, while at 4s the predictions strongly underestimate the observations, which are well above the mean plus one standard deviation. At distances larger than 100 km, the spectral ordinates, recorded mainly at rock/stiff sites, sharply decrease. Similar features can be also found in Iervolino et al. (2012).

Figure 10 shows the comparison between the ITA10 and the observations of the May 29 earthquake considering a larger sample of near-fault observations. The comparison with ITA10 (Figures 10a – 10b) indicates very similar trends to the May 20 event. Observed PGAs and PGVs decay faster than ITA10 at distances larger than about 80 km. At distances less than 10 km, observed PGAs are within the mean minus one standard deviation, while the opposite in observed for PGVs that are within one standard deviation above the mean. These results are in agreement with Bordoni et al. (2012), who used additional data in the near source, collected during a temporary experiment.

Figures 10c and 10d show the vertical PGAs and PGVs compared to the ITA10: the mean predictions for EC8 C site well fit the observed PGAs, except for the record at MRN, above the fault, that is strongly underestimated by the model, as observed by Bordoni et al. (2012) for other near-source stations. In terms of vertical PGV, the ITA10 predictions for EC8 C sites overestimate the observed peak values that decay with distance similarly to the mean for EC8 A sites. These trends suggest that, in the proximity of the source, the high frequency vertical motion is much larger than the Italian mean estimates, but it decays faster, as also observed for the horizontal motion. The

low frequency characteristics of the May 29 event are very similar to those observed for the event of May 20 (Figure 10e and 10f).

In order to quantify the fit of the ITA10 and the MS08 models with the Emilia data, we perform a residual analysis in the period interval 0.1s - 4s. The residuals, expressed as the $\log_{10}$ of the ratio between observed and predicted values, are computed with respect to ITA10 for thrust-fault related events and classifying each site according to the respective class, as in Table 2. For the MS08 no specification of style of faulting was necessary and the sites were discriminated as soil or rock. Figure 11a show the computed residuals, either in function of the moment magnitude or the R_{JB}, at 0.3s and 2.0s for ITA10. The mean residuals for each event are close to zero or slightly negative (i.e., overestimation) and do not show an evident dependence on magnitude. Conversely, a significant dependence on distance is observed: at short periods, the residuals, averaged according to distance-bins, are negative in the range 20 - 80 km, while, in the same distance range, the residuals are slightly positive at 2.0s.

This trend is highlighted in Figure 11b, where the mean residuals are shown for a larger number of distance bins and of a larger period range, between 0.1s and 4s. The mean residuals are negative at short periods (i.e. 0.1s and 0.3s) and positive at long periods (i.e. 2s and 4s) up to 80 km, indicating that the predictions overestimate or underestimate the observations, respectively. In particular, the difference between the over and under estimations at short and long periods is maximized between 20 and 80 km. Stations in this distance range are located in the Po plain, suggesting that path and/or regional site effects can affect the ground motion causing high-frequency attenuation and/or low-frequency amplification. For all the analysed frequencies, a bump in the residuals can be observed at distances of about 120 km. The same feature has been reported by Bragato et al. (2011) for PGA, explained as the reflection of S waves at the Moho (SmS phase), maximized at hypocentral distances between 90 and 150 km. In particular, Bragato et al. (2011) observed a PGA increase by a factor larger than 2.4 with respect to the prediction for the Italian ShakeMaps (Michelini et al., 2008).

In Figure 12a the same comparison as in Figure 11a is made for the MS08. Figure 12a shows the computed residuals, either in function of the moment magnitude or the R_{JB}, at 0.3s and 2.0s. The mean residuals for each event are close to zero at 0.3s and positive (i.e., underestimation) at 2.0s, although do not show an evident dependence on magnitude and distance. As the maximum distance is set at 100 km, the "bump" in the residuals observed for the ITA10 at about 120 km cannot be appreciated. Nevertheless, the standard deviations of the residuals are larger than ITA10.

Figure 12b displays the average residuals in function of the epicentral distance for three periods, 0.1s 0.3s and 2s, as the MS08 is not derived for periods equal to 4s., evidencing that, in general, the MS08 strongly underestimates the observations at all distances at 0.3s, while, at 2s the GMPE underestimates the observations only in the vicinity of the source ($R < 30$ km).

Finally, Figure 13 shows the mean residuals for each station, with respect to ITA10, at different periods. At short periods (0.1s), the GMPE predicts larger motions, except for the *Southern Alps* region (Figures 13a), where the observed high-frequency ground-motion is larger than the predictions, as also shown in Figure 7a. At intermediate periods (1s) there is a general overestimation (Figure 13b), while at long periods (2s and 4s) the ITA10 underestimates the observations for most of the stations in the Po plain (white dots in the Figures 13c and 13d) while overestimates the ground motion for the stations located in the western Northern Apennines and at the border of the *Southern Alps* (black squares in Figures 13c and 13d).

7. CONCLUSION

During the 2012 Emilia seismic sequence, for the first time in Italy after the 1976 Friuli earthquakes, moderate to strong earthquakes were recorded in northern Italy. The 2012 sequence is located in the Po plain, a sedimentary basin, covering an area of about 50.000 km^2, characterized by variable sediment thickness, ranging from several kilometres to tens of meters. The geologic conditions characterizing the Po plain region are unique in the Italy and there are very few similar

contexts worldwide (i.e. Los Angeles basin, Kanto basin, although of smaller extension), therefore the Emilia strong-motion records are of major relevance, since they increase the worldwide data set of strong motion recorded in very deep sedimentary structures. Moreover, in Italy they fill the gap of compressive (thrust-fault) events recorded on very deep soft sites, increasing the data set used to derive the Italian ground-motion prediction equations (Bindi et al., 2011).

In the Po plain, the trapping and the conversion of the body waves in the thick sedimentary cover, causes the generation of surface waves, which dominate the seismic signals, at periods longer than 2s. At distances larger than 30 km, peak velocities and displacements generally occur in correspondence of the surface waves and an extreme lengthening of the signals can be observed. At large distances (> 150 km) 5s surface waves are still evident from NNE Italy to SSW, for the two strongest events.

The spatial distribution of the ground motion of the two strongest events shows a correlation with the local and regional geological setting. The area characterized by the largest spectral ordinates at long periods (> 4 s) depicts the limits of the deepest and youngest Po plain sediments (Emilia-Romagna and Venetian plain). At the same time, long period ground motion strongly attenuates to the SW, in correspondence of the northern Apennines and to the S of the Ferrara arc, while the largest amplitudes are recorded in the part of the Po plain confined between the outer structures of this arc and the Northern Apennines mountain front.

These features are probably the cause the following discrepancies with the expected mean ground motion for the Italian territory, predicted by the ITA10: i) enhanced long period (> 1s) spectral amplitudes for the horizontal components of the sites located in Po plain; ii) higher short-period content in the vertical motion in the proximity of the source and faster high frequency attenuation at distances larger than the source dimension for both horizontal and vertical components; iii) higher attenuation, after 80 km, of the spectral ordinates at period longer than 0.1 s; iv) relative enhancement of spectral ordinates at distances of about 120 km, particularly evident for short periods (0.1 s).

These discrepancies underline the need of deriving a specific GMPE for the Po plain area, especially for the long period range (T > 1s).

DATA AND RESOURCES

The INGV strong motion data, recorded during the Emilia seismic sequence, by the permanent stations and some temporary stations, are released through the INGV strong motion data web portals (http://www.mi.ingv.it/ISMD/ismd and http://dyna.mi.ingv.it/DYNA-archive).

The raw strong-motion data recorded by the RAN, are available on the web-site of the Italian Department of Civil Protection (http://www.protezionecivile.it).

Event origin times and locations are published on the Italian Seismic Instrumental and parametric Data-basE, IsidE (http://iside.rm.ingv.it).

Additional information on site classification adopted for the strong-motion stations can be found on the Italian strong motion database (http://itaca.mi.ingv.it).

ACKNOWLEDGEMENTS

The authors acknowledge the referee, Alberto Michelini, for the valuable contribution in improving the quality of this paper. The authors extend their gratitude to D. Bindi for his help in the discussion on the residual analysis results.

REFERENCES

Amorosi, A., L. Caporale, U. Cibin, M. L. Colalongo, G. Pasini, F. Ricci Lucchi, P. Severi, and S. Vaiani (1998). The Pleistocene littoral deposits (Imola Sands) of the Northern Apennines foothills, *Giornale di Geologia*, **60**, 83-118.

Bartolini, C., R. Caputo, and M. Pieri (1996). Pliocene-Quaternary sedimentation in the Northern Apennine foredeep and related denudation, *Geological Magazine*, **133**, 255-273.

Bigi, G., G. Bonardi, R. Catalano, D. Cosentino, F. Lentini, M. Parotto, R. Sartori, P. Scandone, and E. Turco (Eds.) (1992). Structural Model of Italy and gravity map, *Quaderni della Ricerca Scientifica*, **114,** C.N.R. Progetto Finalizzato Geodinamica.

Bindi, D., F. Pacor, L. Luzi, R. Puglia, M. Massa, G. Ameri and R. Paolucci (2011). Ground motion prediction equations derived from the Italian strong motion database, *Bulletin of Earthquake Engineering*, **9**, 1899-1920; doi: 10.1007/

Boore, D. M., and J. J. Bommer (2005). Processing of strong-motion accelerograms: Needs, options and consequences, *Soil Dynamics and Earthquake Engineering*, **25**, 93-115.

Bordoni P., R. M. Azzara, F. Cara, R. Cogliano, G. Cultrera, G. Di Giulio, A. Fodarella, G. Milana, S. Pucillo, G. Riccio, A. Rovelli, P. Augliera, L. Luzi, S. Lovati, M. Massa, F. Pacor, R. Puglia and G. Ameri (2012). Preliminary results from EMERSITO, a rapid response network for site-effect studies, *Annals of Geophysics*, "The Emilia (northern Italy) seismic sequence of May-June, 2012: preliminary data and results", Anzidei M., Maramai A. and Montone P. (Eds), **55**, 4, in press.

Bragato, P. L., Sugan, M. Augliera, P. Massa, M., Vuan, A. and A. Sarao (2011). Moho Reflection Effects in the Po Plain (Northern Italy) Observed from Instrumental and Intensity Data. *Bulletin of the Seismological Society of America*, **101(5)**, 2142–2152. doi:10.1785/0120100257

Burrato, P., P. Vannoli, U. Fracassi, R. Basili, and G. Valensise (2012). Is blind faulting truly invisible? Tectonic-controlled drainage evolution in the epicentral area of the May 2012, Emilia-Romagna

earthquake sequence (northern Italy), *Annals of Geophysics*, "The Emilia (northern Italy) seismic sequence of May-June, 2012: preliminary data and results", Anzidei M., Maramai A. and Montone P. (Eds), **55**, 4, in press.

Burrato P., Ciucci F., Valensise G. (2003). An inventory of river anomalies in the Po plain, Northern Italy: evidence for active blind thrust faulting, Annals of Geophysics, **46 (5)**, 865-882.

Capozzi, R., and V. Picotti (2003). Pliocene sequence stratigraphy, climatic trends and sapropel formation in the Northern Apennines (Italy), *Palaeogeography Palaeoclimatology Palaeoecology*, **190**, 349-371.

Carminati, E., D. Scrocca, and C. Doglioni (2010). Compaction-induced stress variations with depth in an active anticline: Northern Apennines, Italy, *J. Geophys. Res.*, **115**, B02401, doi:10.1029/2009JB006395.

Carminati, E., and C. Doglioni (2012). Alps Vs. Apennines: The paradigm of a tectonically asymmetric Earth, *Earth Science Review*, **112**, 67-96, doi:10.1016/ j.earscirev.2012.02.004.

Cassano, E., L. Anelli, R. Fichera, and V. Cappelli (1986). Pianura Padana – Interpretazione integrata di dati geofisici e geologici. 73° Congresso Società Geologica Italiana, 29 Settembre-4 Ottobre 1986, Roma, 27 pp.

Castellarin, A., and L. Cantelli (2000). Neo-Alpine evolution of the Southern Eastern Alps, *Journal of Geodynamics*, **30**, 251-274.

Castello, B., G. Selvaggi, C. Chiarabba, and A. Amato (2006). CSI Catalogo della sismicità italiana 1981-2002, versione 1.1. INGV-CNT, Roma http://www.ingv.it/CSI/.

Comité Européen de Normalisation (CEN) (2004). Eurocode 8: Design of Structures for Earthquake Resistance—Part 1: General Rules, Seismic Actions and Rules for Buildings. Brussels: Comité Européen de Normalisation.

Davis, J. C. (1973). Statistics and Data Analysis in Geology. New York: Wiley, 550 pp..

Desio, A. (1965). I rilievi isolati della Pianura Lombarda ed i movimenti tettonici del Quaternario, *Rendiconti Istituto Lombardo Accademia Scienze Lettere*, Sez. A 99, 881-894.

Devoti, R., A. Esposito, G. Pietrantonio, A. R. Pisani, and F. Riguzzi (2011). Evidence of large scale deformation patterns from GPS data in the Italian subduction boundary, *Earth and Planetary Science Letters*, **311**, 3–4, 230-241, doi:10.1016/j.epsl.2011.09.034.

Di Capua, G., G. Lanzo, V. Pessina, S. Peppoloni, and G. Scasserra (2011). The recording stations of the Italian strong motion network: geological information and site classification, *Bulletin of Earthquake Engineering*, **9**, 1779-1796, doi:10.1007/s10518-011-9326-7.

DISS Working Group (2010), Database of Individual Seismogenic Sources (DISS), Version 3.1.01: A compilation of potential sources for earthquakes larger than M 5.5 in Italy and surrounding areas, http://diss.rm.ingv.it/diss/.

Fantoni, R., and R. Franciosi (2010). Tectono-sedimentary setting of the Po Plain and Adriatic Foreland, *Rendiconti Fisici Accademia Lincei*, **21**, 1, 197-209, doi: 10.1007/s12210-010-0102-4.

Hanks, T. C. (1975). Strong ground motion of the San Fernando, California, earthquake: ground displacements, *Bulletin of the Seismological Society of America*, **65**, 193–225.

Hisada Y., K. Aki, T. Teng (1993). Application of Nonstationary Ray Decomposition to Identifying Deep Seismic Bedrock of the Kanto Sedimentary Basin, Japan. Bulletin of the Seismological Society of America, Vol. 83, No. 6, pp. 1700 1720, December 1993

Iervolino I., F. De Luca, E. Chiocarelli (2012). Engineering seismic demand in the 2012 Emilia sequence: preliminary analysis and model compatibility assessment. Annals of Geophysics *Annals of Geophysics*, "The Emilia (northern Italy) seismic sequence of May-June, 2012: preliminary data and results", Anzidei M., Maramai A. and Montone P. (Eds), **55**, 4, in press.

Joyner W. B. (2000). Strong Motion from Surface Waves in Deep Sedimentary Basin. Bulletin of the Seismological Society of America, vol. 90 (6B), S95-S112.

Kagawa, T., B. Zhao, K. Miyakoshi, and K. Irikura (2004). Modeling of 3D Basin Structures for Seismic Wave Simulations Based on Available Information on the Target Area: Case Study of the Osaka Basin, Japan. *Bulletin of the Seismological Society of America*, **94**, 4, 1353-1368.

Livio, F.A., A. Berlusconi, A. M. Michetti, G. Sileo, A. Zerboni, L. Trombino, M. Cremaschi, K. Mueller, E. Vittori, C. Carcano, and S. Rogledi (2009). Active fault-related folding in the epicentral area of the December 25, 1222 (Io = IX MCS) Brescia earthquake (Northern Italy): seismotectonic implications, *Tectonophysics*, **476**, 1-2, 320-335, doi:10.1016/j.tecto.2009.03.019.

Malagnini, L., R. B. Herrmann, I. Munafò, M. Buttinelli, M. Anselmi, A. Akinci, and E. Boschi (2012). The 2012 Ferrara seismic sequence: regional crustal structure, earthquake sources, and seismic hazard, Geophysical Research Letters,doi:10.1029/2012GL053214, in press.

Mariotti, G., and C. Doglioni (2000). The dip of the foreland monocline in the Alps and Apennines, *Earth and Planetary Science Letters*, **181**, 191-202.

Michelini, A., L. Faenza, V. Lauciani, and L. Malgnini (2008). ShakeMap Implementation in Italy, *Seismol. Res. Lett.* **79**, 688–697.

Montone, P., M. T. Mariucci, and S. Pierdominici (2012). The Italian present-day stress map, *Geophysical Journal International*, **189**, 705-716, doi: 10.1111/j.1365-246X.2012.05391.x.

Morasca, P., M. Massa, E. Laprocina, K. Mayeda, S. Phillips, L. Malagnini, D. Spallarossa G. Costa and P. Augliera (2010). Improved 2-D attenuation analysis for Northern Italy using a merged dataset from selected regional seismic networks. Journal of Seismology, 14(4), 727–738. doi:10.1007/s10950-010-9194-7

Pacor, F., R. Paolucci, G. Ameri, M. Massa, and R. Puglia (2011). Italian strong motion records in ITACA: overview and record processing, *Bulletin of Earthquake Engineering*, **9**, 1741-1759.

Paolucci R, Pacor F, Puglia R, Ameri G, Cauzzi C and Massa M (2011) Record processing in ITACA, the new Italian strong-motion database. In: Akkar S, Gulkan P, Van Eck T (eds) Earthquake data in

engineering seismology, geotechnical, geological and earthquake engineering series, vol 14, Chapter 8, pp 99–113. Springer, Berlin.

Pinnegar, C. (2006). Polarization analysis and polarization filtering of three-component signals with the time-frequency S-transform, *Geophysical Journal International*, **165**, 2, 596-606.

Pondrelli, S., A. Morelli, G. Ekström, S. Mazza, E. Boschi, and A. M. Dziewonski (2002). European-Mediterranean regional centroid-moment tensors: 1997-2000, Phys. Earth Planet. Int., **130**, 71-101.

Pondrelli, S., S. Salimbeni, G. Ekstrom, A. Morelli, P. Gasperini, and G. Vannucci (2006). The Italian CMT dataset from 1977 to the present, *Physics of the Earth and Planetary Interior*, **159**, 3-4, 286-303, doi:10.1016/j.pepi.2006.07.008.

Pondrelli, S., G. Ekstrom, and A. Morelli (2001), Seismotectonic re-evaluation of the 1976 Friuli, Italy, seismic sequence, J Seismol, 5, 78–83.

Pondrelli, S., S. Salimbeni, P. Perfetti, and P. Danecek (2012). Quick regional centroid moment tensor solutions for the Emilia 2012 (northern Italy) seismic sequence, *Ann. Geophys.*, 55, 4, doi: 10.4401/ag-6146.

R.E.R, and ENI-AGIP (1998). Riserve idriche sotterranee nella Regione Emilia-Romagna, Di Dio, G. (Ed), S.EL.CA., Firenze ,119 pp., 9 sheets.

Rovida, A., R. Camassi, P. Gasperini, and M. Stucchi (Eds.) (2011). CPTI11, the 2011 version of the Parametric Catalogue of Italian Earthquakes. Milano, Bologna, available at: http://emidius.mi.ingv.it/CPTIhttp://emidius.mi.ingv.it/CPTI.

Salvaterra, L., S. Pintore, L. Badiali (2008) Rete sismologica basata su stazioni GAIA. Rapporti Tecnici INGV n. 68, 26 pp.

Sato, T., R. W. Graves, and P. G. Somerville (1999). Three-dimensional finite-difference simulations of long-period strong motions in the Tokyo metropolitan area during the 1990 Odawara earthquake (MJ

5.1) and the Great 1923 Kanto earthquake (MS 8.2) in Japan, *Bulletin of the Seismological Society of* America, **89**, 579–607.

Scognamiglio, L., L. Margheriti, F. M. Mele, E. Tinti, A. Bono, P. De Gori, V. Lauciani, F. P. Lucente, A. G. Mandiello, C. Marcocci, S. Mazza, S. Pintore, and M. Quintiliani (2012). The 2012 Pianura Padana Emiliana Seimic Sequence: Locations and Magnitudes. *Annals of Geophysics*, "The Emilia (northern Italy) seismic sequence of May-June, 2012: preliminary data and results", Anzidei M., Maramai A. and Montone P. (Eds), **55**, 4, in press.

Somerville, P. G., N. F. Collins, R. W. Graves, and A. Pitarka (2004). An engineering ground motion model for basin generated surface waves, Proc. 13th World Conference on Earthquake Engineering, Vancouver, Canada, Paper 515.

Stockwell R.G., L. Mansinhaand and R. P. Lowe (1996). Localization of the complex spectrum: The S transform, *IEEE Trans Signal Process*, **44**, 998–1001.

Steidl, J. H., and Y. Lee (2000). The SCEC phase III strong-motion database, *Bulletin of the Seismological Society of* America, **90**, S113–S135.

Captions

Table 1. Location and magnitude of the 6 strongest events (* = INGV, http://iside.rm.ingv.it/ ; ** = Regional Centroid Moment Tensor http://www.bo.ingv.it/RCMT/)

Table 2. Main features of the strong motion recording stations.

Figure 1. a) Simplified geological sketch of the Po plain and surrounding Northern Apennines and Southern Alps fold-and-thrust belts. Key to symbols: stars, earthquakes of M > 5 of the 2012 Emilia-Romagna seismic sequence, dimension proportional to the magnitude; dark grey areas, Composite Seismogenic Sources (CSS) of the DISS database (http://diss.rm.ingv.it), the upper tip of the fault plane is highlighted in black. Focal mechanisms of the 20 and 29 May 2012 earthquakes are from the TDMT database (http://cnt.rm.ingv.it/tdmt.html). b) Simplified geological sections crossing the Po plain and showing thickness variation of the Plio-Quaternary sedimentary sequence correlated with syncline-anticlines pairs of the Northern Apennines and Southern Alps thrust belts. Modified from Cassano et al. (1986), sections 1, 2 and 3; Livio et al. (2009), section 1 and Carminati et al. (2010), section 2.

Figure 2. Left: magnitude distribution of the records relative to the 6 examined events, compared to the data set used to derive the Bindi et al. (2011) for compressive events in Italy. Right: magnitude-distance distribution. White indicates records prior to the Emilia sequence; grey indicates the records relative to the 6 events.

Figure 3. Map of the recording stations superimposed on the recent deposits of the Po plain (all the instruments are accelerometers).

Figure 4. Left: vertical and NS component of the acceleration and velocity time histories of the station MOG0; Right: vertical and NS component of the acceleration and velocity time histories of the station OPPE. Grey shaded areas indicate surface waves.

Figure 5. Left: acceleration time series recorded at Mirandola (MRN); Right: acceleration time series recorded at Modena (MODE). Grey shaded areas identify the interval within 5% and 95% of the total Arias intensity

Figure 6. Velocity time series plots of the NS component and total power spectra of 10 selected stations (the amplitudes of the total power spectra are expressed in cm).

Figure 7. Maps of the interpolated ground motion parameters (geometric mean of the horizontal components): a) PGA May 20th; b) PGA May 29th; c) PGV May 20th; d) PGV May 29th; e) PGD May 20th; d) PGD May 29th. Green lines are the border of the Plio-Quaternary sediments, red lines are the main tectonic features and blue lines are the limits of the Trento carbonatic platform.

Figure 8. Maps of the interpolated acceleration spectral ordinates (geometric mean of the horizontal components): a) T = 1.0s May 20th; b) T = 1.0s May 29th; c) T = 4.0s May 20th; d) T = 4.0s May 29th; e) T = 10.0s May 20th; d) T = 10.0s May 29th. Green lines are the border of the Plio-Quaternary sediments, red lines are the main tectonic features and blue lines are the limits of the Trento carbonatic platform.

Figure 9. Comparison between predictions (Bindi et al., 2011) and observations relevant to the May 20th event: a) horizontal PGA; b) horizontal PGV; c) vertical PGA; d) vertical PGV; e) acceleration spectral ordinates at T = 2s; f) acceleration spectral ordinates at T = 4s. The ground motion is the geometric mean between the horizontal components. Black solid line is the mean prediction, while

black dashed lines indicate the mean plus/minus one standard deviation for class A; the grey solid line is the mean prediction, while grey dashed lines indicate the mean plus/minus one standard for class C; black dots are the observations for class A; grey dots are the observations for class C.

Figure 10. Comparison between predictions (Bindi et al., 2011) and observations relevant to the May 29th event: a) horizontal PGA; b) horizontal PGV; c) vertical PGA; d) vertical PGV; e) acceleration spectral ordinates at T = 2s; f) acceleration spectral ordinates at T = 4s. The ground motion is the geometric mean between the horizontal components. Black solid line is the mean prediction, while black dashed lines indicate the mean plus/minus one standard deviation for class A; the grey solid line is the mean prediction, while grey dashed lines indicate the mean plus/minus one standard for class C; black dots are the observations for class A; grey dots are the observations for class C.

Figure 11. ITA10: a) Residuals averaged according to magnitude (top panel) and distance (lower panel) bins; b) mean residuals at different periods in function of distance.

Figure 12. MS08: a) Residuals averaged according to magnitude (top panel) and distance (lower panel) bins; b) mean residuals at different periods in function of distance.

Figure 13. Residuals between observed and predicted spectral ordinates: a) T = 0.1 s; b) T =1 s; c) T =2 s; c) T =4 s. Black squares are negative residuals (i.e overestimation of the model), white circles are positive residuals (i.e underestimation of the model). The size of the symbols is proportional to the magnitude of the residuals.

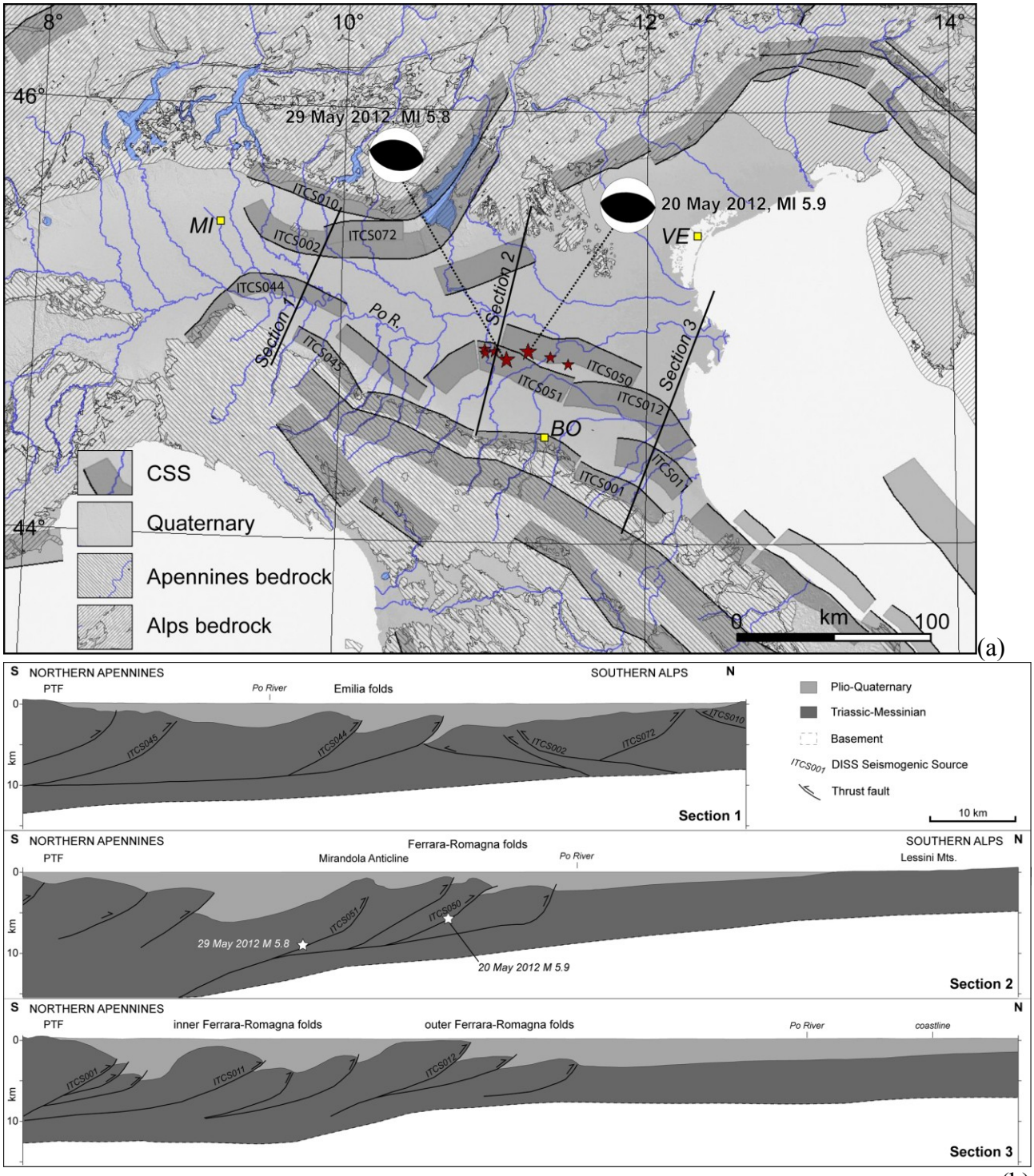
8°
10°
12°
14°
46°
44°
29 May 2012, MI 5.8
20 May 2012, MI 5.9
MI
VE
BO
ITCS010
ITCS072
ITCS002
ITCS044
ITCS045
ITCS050
ITCS051
ITCS012
ITCS001
ITCS011
Section 1
Section 2
Section 3
Po R.
CSS
Quaternary
Apennines bedrock
Alps bedrock
0
km
100
(a)
S
N
NORTHERN APENNINES
SOUTHERN ALPS
PTF
Po River
Emilia folds
Plio-Quaternary
Triassic-Messinian
Basement
DISS Seismogenic Source
Thrust fault
10 km
Section 1
Ferrara-Romagna folds
Mirandola Anticline
Lessini Mts.
29 May 2012 M 5.8
20 May 2012 M 5.9
Section 2
inner Ferrara-Romagna folds
outer Ferrara-Romagna folds
coastline
Section 3
(b)

Figure 1.

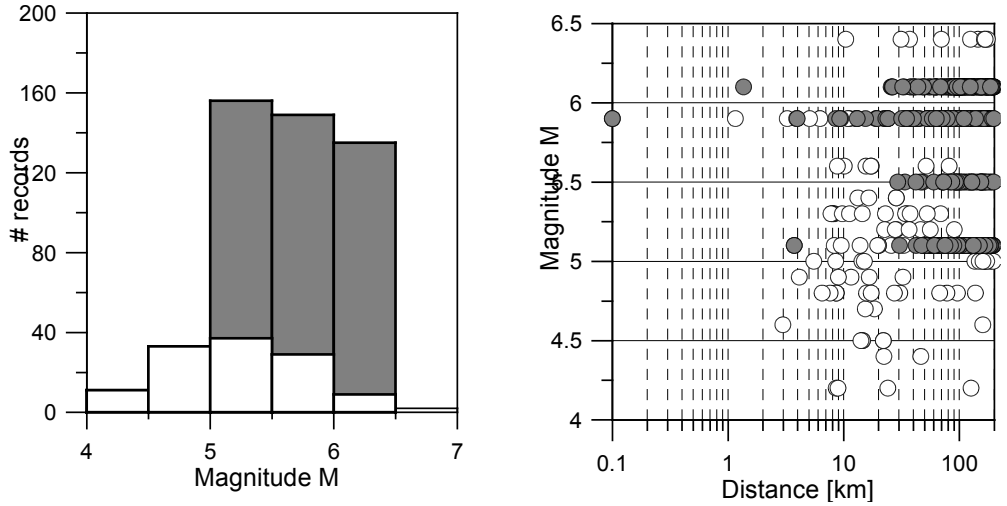
200
160
120
80
40
0
records
4
5
6
7
Magnitude M
6.5
6
5.5
5
4.5
4
Magnitude M
0.1
1
10
100
Distance [km]

Figure 2.

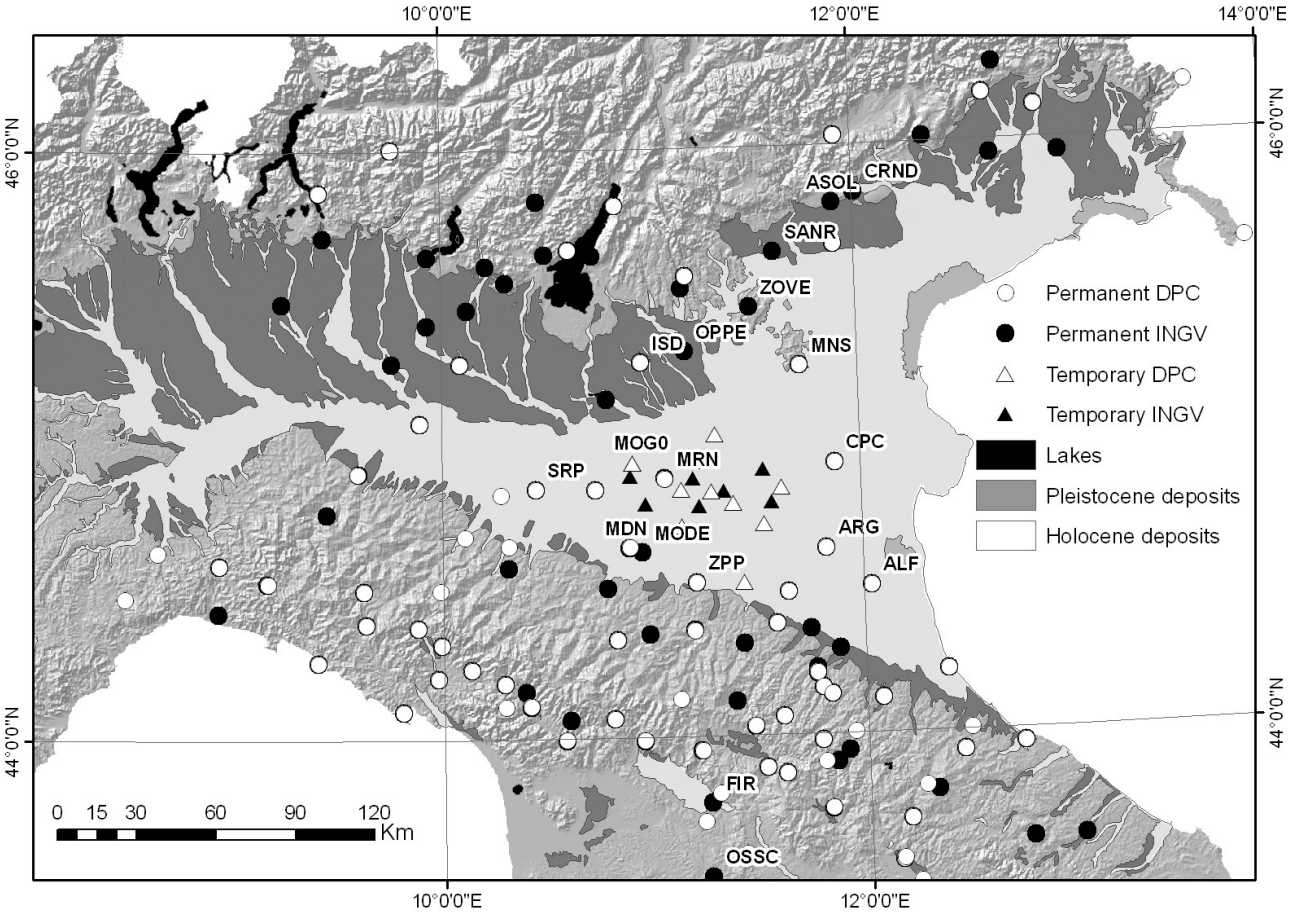
10°0'0"E
12°0'0"E
14°0'0"E
46°0'0"N
44°0'0"N
ASOL
CRND
SANR
ZOVE
OPPE
ISD
MNS
MOG0
MRN
SRP
CPC
MDN
MODE
ARG
ZPP
ALF
FIR
OSSC
Permanent DPC
Permanent INGV
Temporary DPC
Temporary INGV
Lakes
Pleistocene deposits
Holocene deposits
0 15 30 60 90 120
Km

Figure 3.

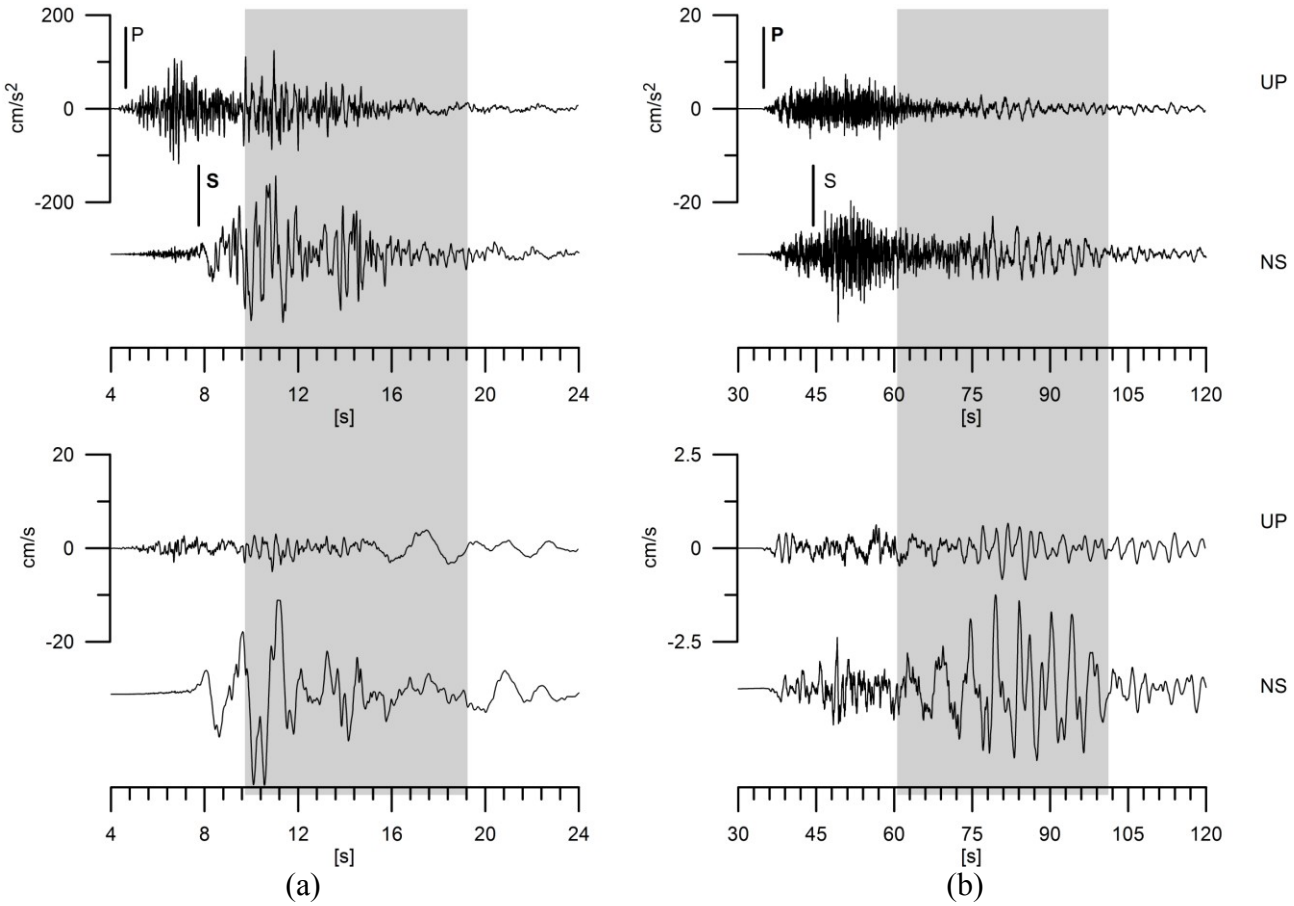
200
P
cm/s2
0
S
-200
4
8
12
16
20
24
[s]
20
cm/s
0
-20
4
8
12
16
20
24
[s]
(a)
20
P
cm/s2
0
S
-20
UP
NS
30
45
60
75
90
105
120
[s]
2.5
cm/s
0
-2.5
UP
NS
30
45
60
75
90
105
120
[s]
(b)

Figure 4.

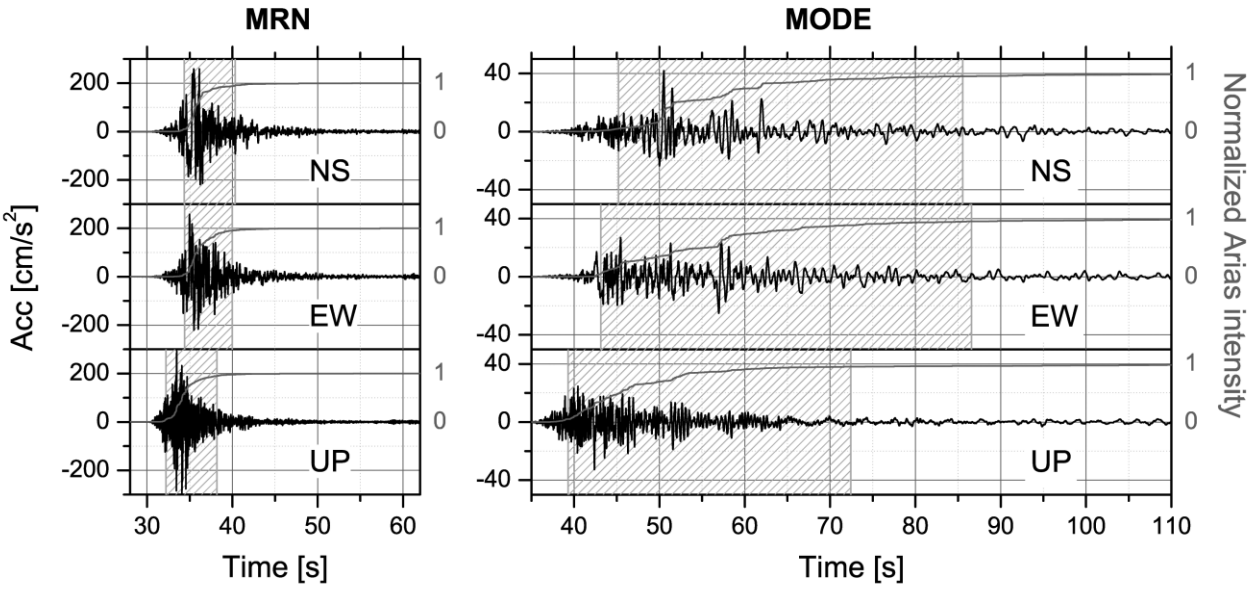

Figure 5.

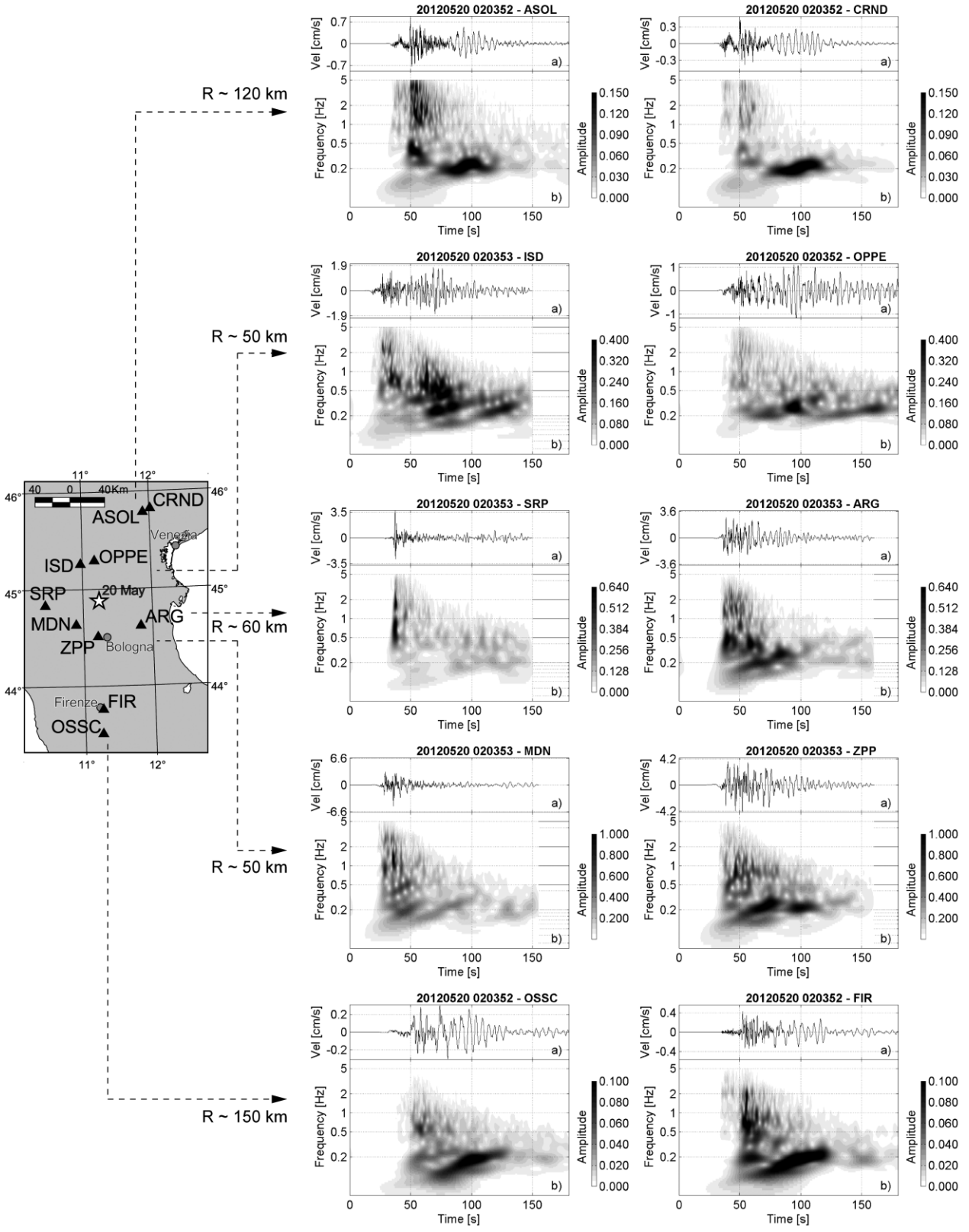
R ~ 120 km
R ~ 50 km
R ~ 60 km
R ~ 50 km
R ~ 150 km
11°
12°
46°
45°
44°
40 0 40Km
CRND
ASOL
Venezia
ISD
OPPE
SRP
20 May
MDN
ARG
ZPP
Bologna
Firenze
FIR
OSSC
20120520 020352 - ASOL
20120520 020352 - CRND
20120520 020353 - ISD
20120520 020352 - OPPE
20120520 020353 - SRP
20120520 020353 - ARG
20120520 020353 - MDN
20120520 020353 - ZPP
20120520 020352 - OSSC
20120520 020352 - FIR
Vel [cm/s]
Frequency [Hz]
Amplitude
Time [s]
a)
b)

Figure 6.

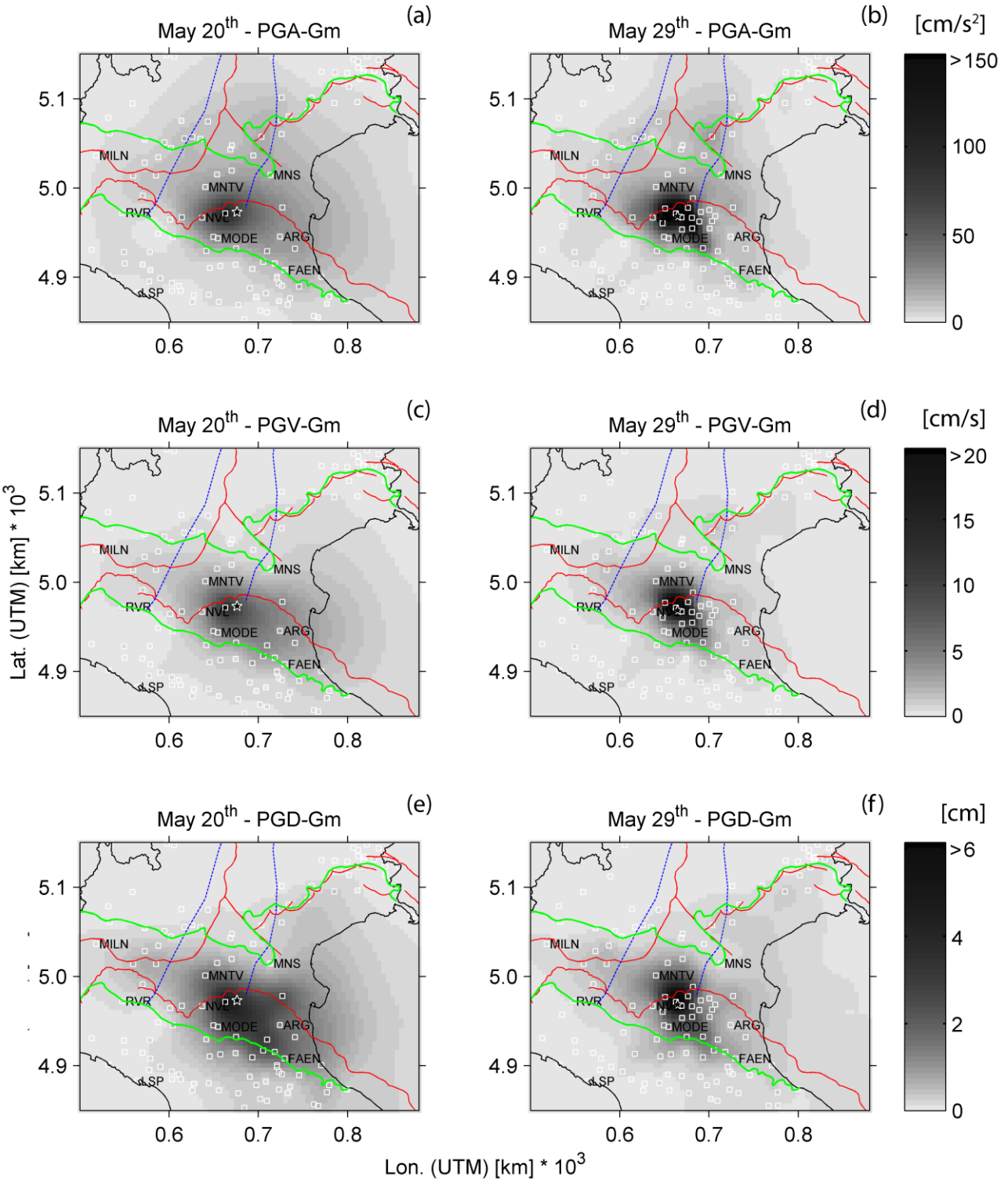
(a)
May 20th - PGA-Gm
(b)
May 29th - PGA-Gm
[cm/s²]
>150
100
50
0
(c)
May 20th - PGV-Gm
(d)
May 29th - PGV-Gm
[cm/s]
>20
15
10
5
0
(e)
May 20th - PGD-Gm
(f)
May 29th - PGD-Gm
[cm]
>6
4
2
0
MILN
MNS
MNTV
RVR
NVL
MODE
ARG
FAEN
SP
5.1
5.0
4.9
0.6
0.7
0.8
Lat. (UTM) [km] * 10³
Lon. (UTM) [km] * 10³

Figure 7.

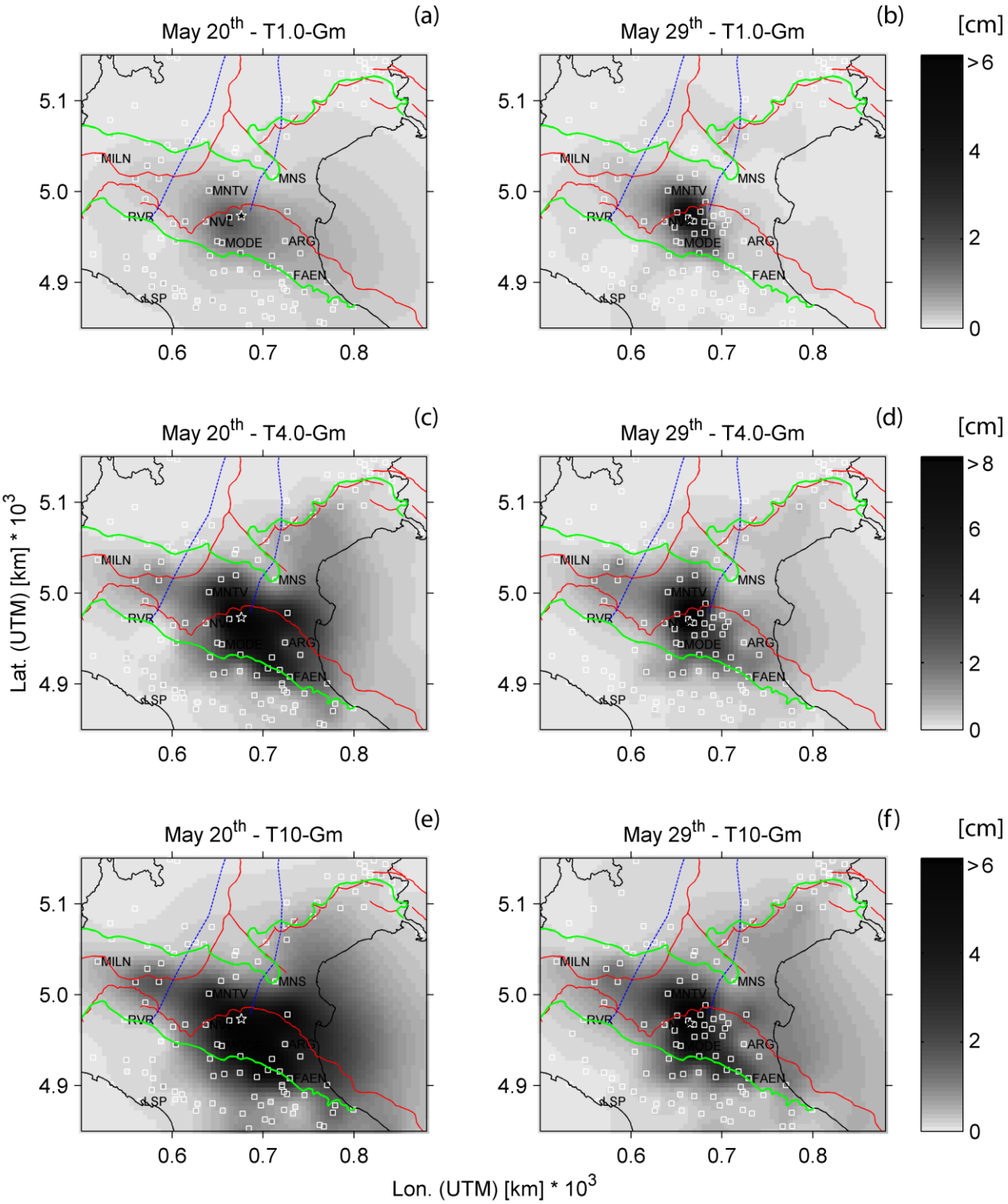
(a)
May 20th - T1.0-Gm
(b)
May 29th - T1.0-Gm
[cm]
>6
4
2
0
(c)
May 20th - T4.0-Gm
(d)
May 29th - T4.0-Gm
[cm]
>8
6
4
2
0
(e)
May 20th - T10-Gm
(f)
May 29th - T10-Gm
[cm]
>6
4
2
0
MILN
MNS
MNTV
RVR
NVE
MODE
ARG
FAEN
SP
5.1
5.0
4.9
0.6
0.7
0.8
Lat. (UTM) [km] * 10^3
Lon. (UTM) [km] * 10^3

Figure 8.

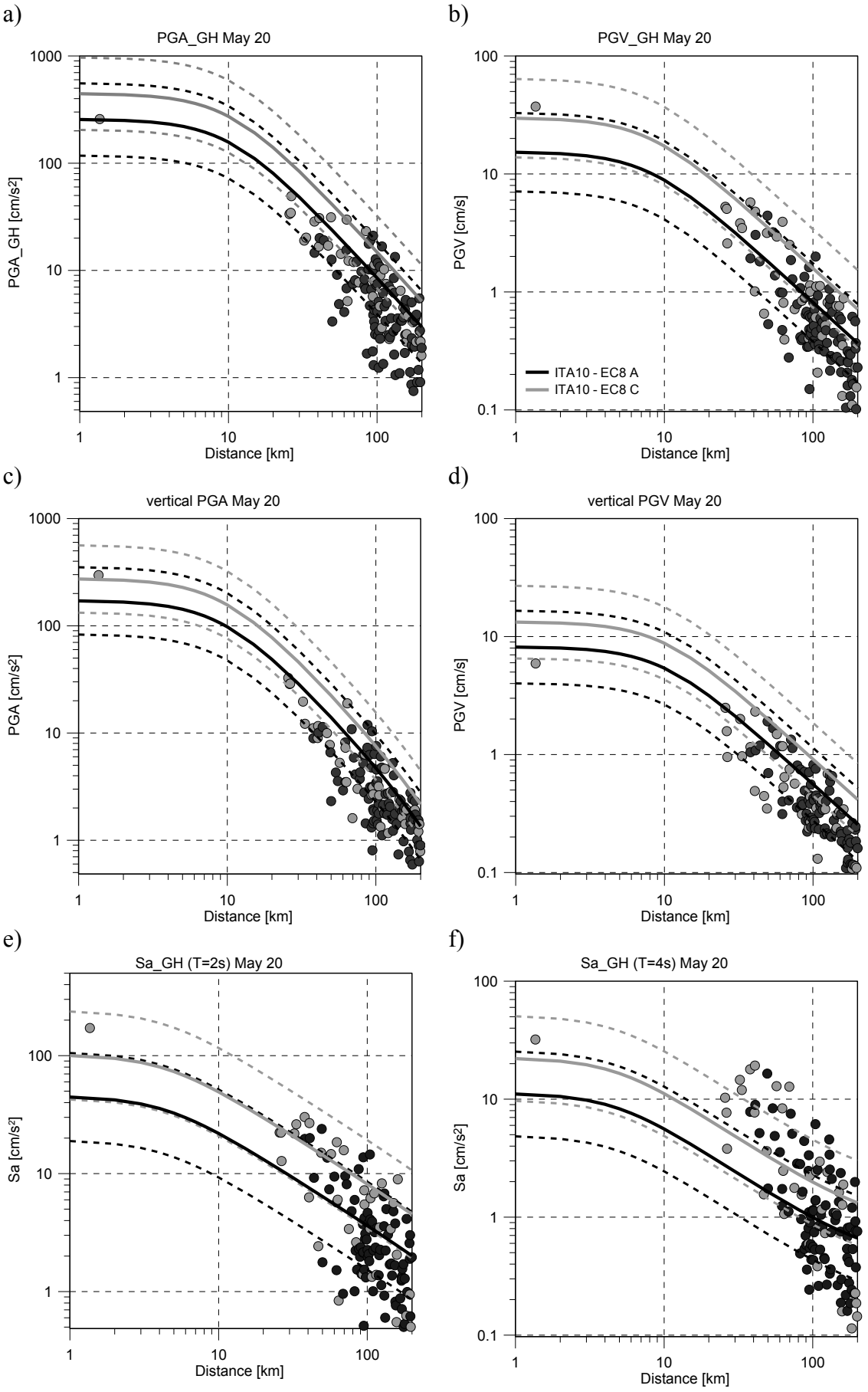
a)
PGA_GH May 20
PGA_GH [cm/s²]
Distance [km]
b)
PGV_GH May 20
PGV [cm/s]
ITA10 - EC8 A
ITA10 - EC8 C
Distance [km]
c)
vertical PGA May 20
PGA [cm/s²]
Distance [km]
d)
vertical PGV May 20
PGV [cm/s]
Distance [km]
e)
Sa_GH (T=2s) May 20
Sa [cm/s²]
Distance [km]
f)
Sa_GH (T=4s) May 20
Sa [cm/s²]
Distance [km]

Figure 9.

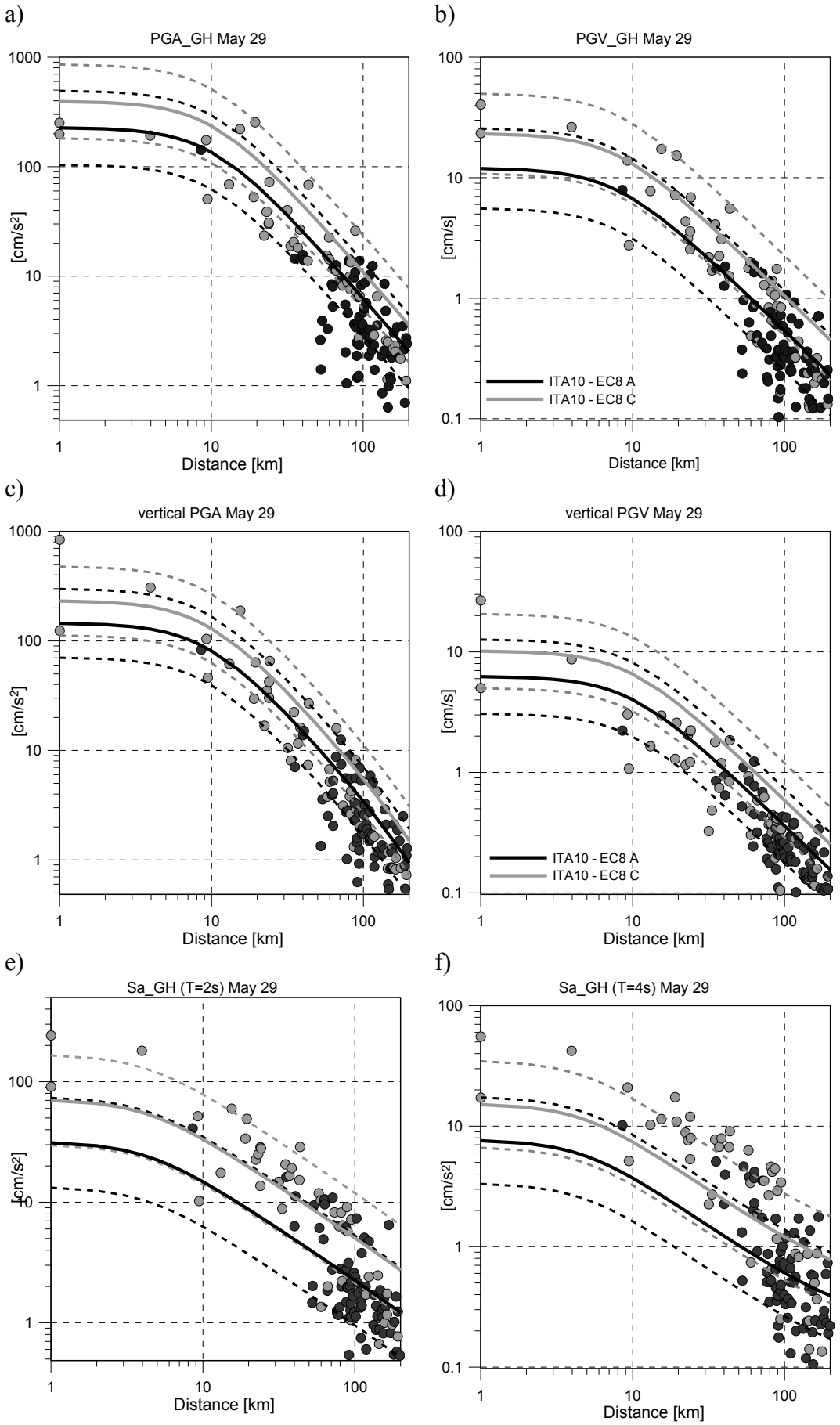
a)
PGA_GH May 29
[cm/s²]
Distance [km]
b)
PGV_GH May 29
[cm/s]
Distance [km]
ITA10 - EC8 A
ITA10 - EC8 C
c)
vertical PGA May 29
[cm/s²]
Distance [km]
d)
vertical PGV May 29
[cm/s]
Distance [km]
ITA10 - EC8 A
ITA10 - EC8 C
e)
Sa_GH (T=2s) May 29
[cm/s²]
Distance [km]
f)
Sa_GH (T=4s) May 29
[cm/s²]
Distance [km]

Figure 10.

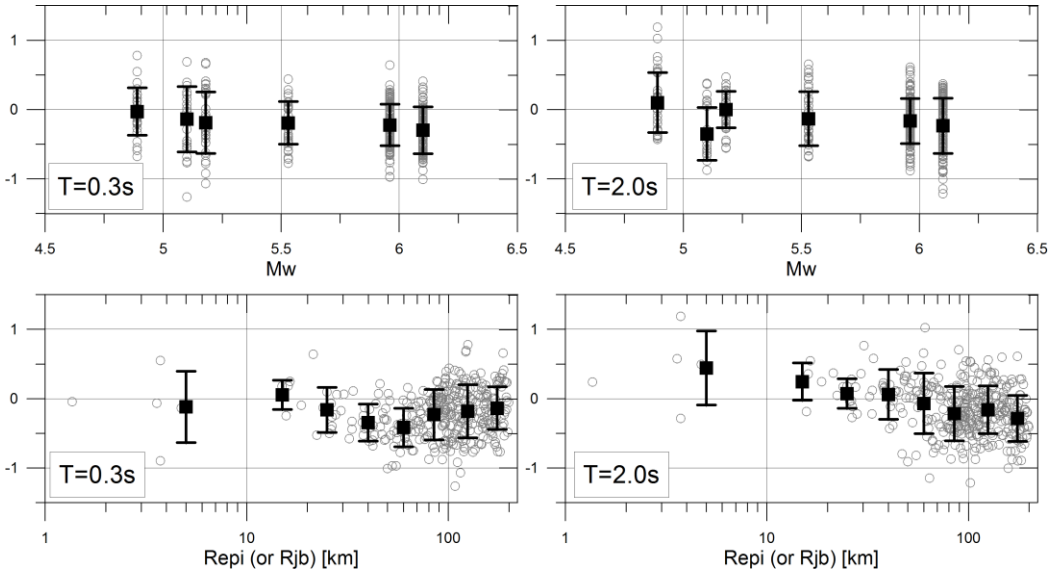
T=0.3s
T=2.0s
Mw
Repi (or Rjb) [km]

(a)

(b)

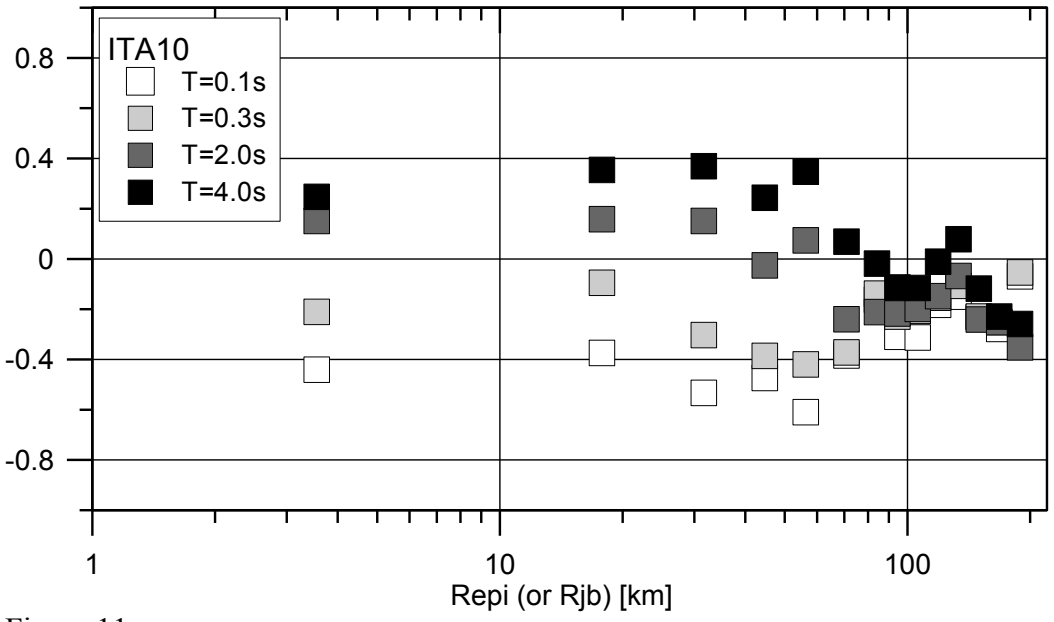
ITA10
T=0.1s
T=0.3s
T=2.0s
T=4.0s
Repi (or Rjb) [km]

Figure 11.

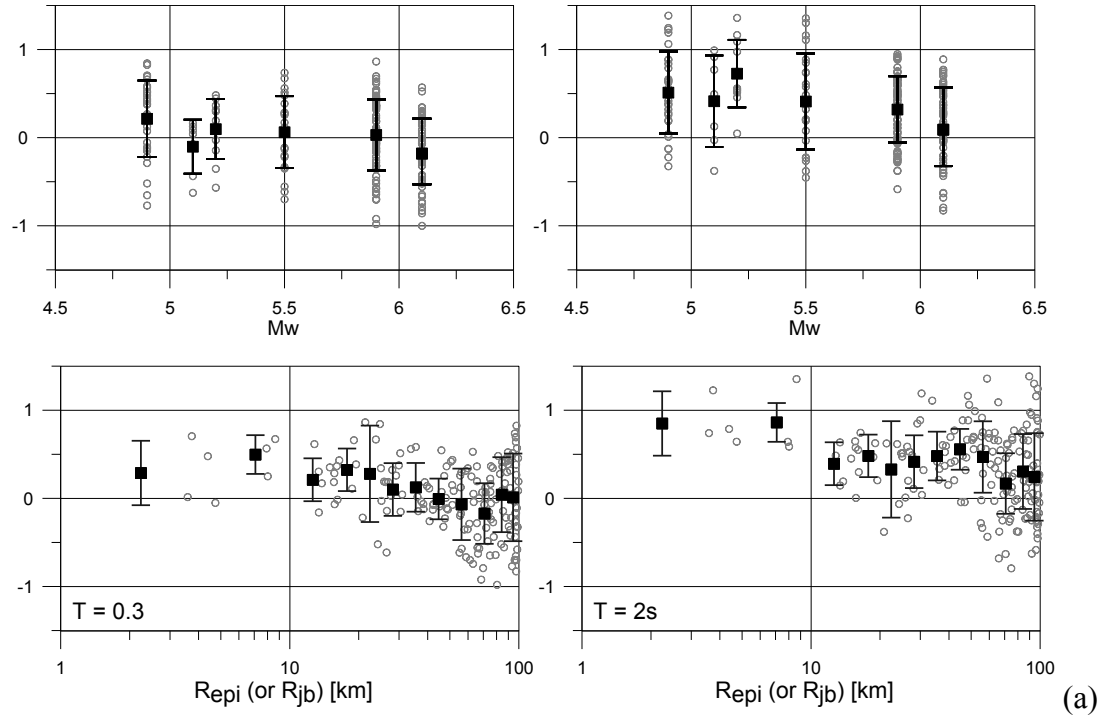
1
0
-1
4.5
5
5.5
6
6.5
Mw
T = 0.3
T = 2s
1
10
100
Repi (or Rjb) [km]

(a)

(b)

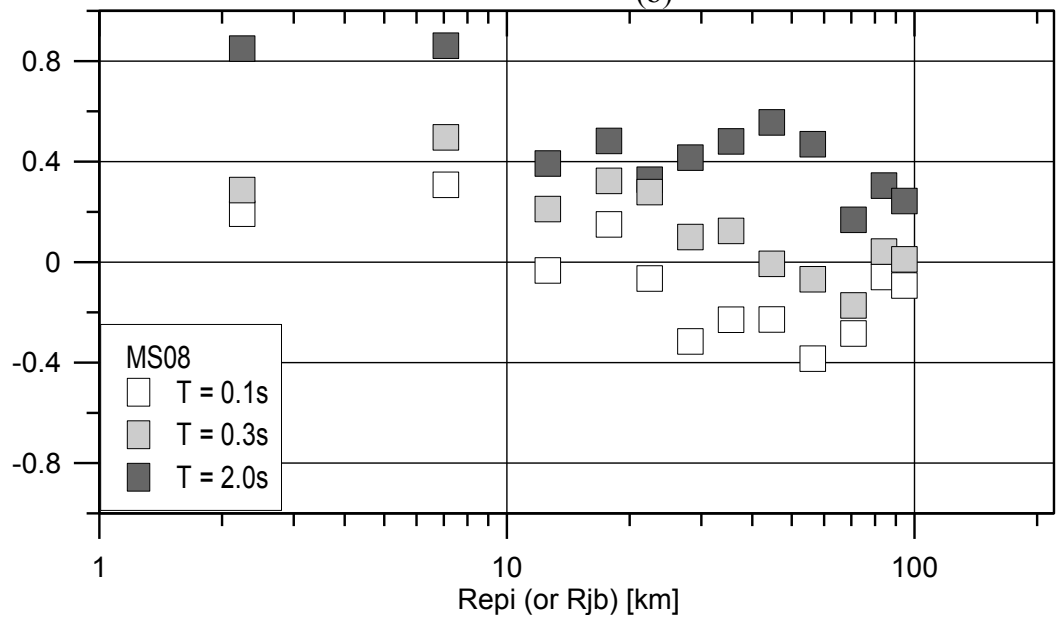
0.8
0.4
0
-0.4
-0.8
MS08
T = 0.1s
T = 0.3s
T = 2.0s
1
10
100
Repi (or Rjb) [km]

Figure 12

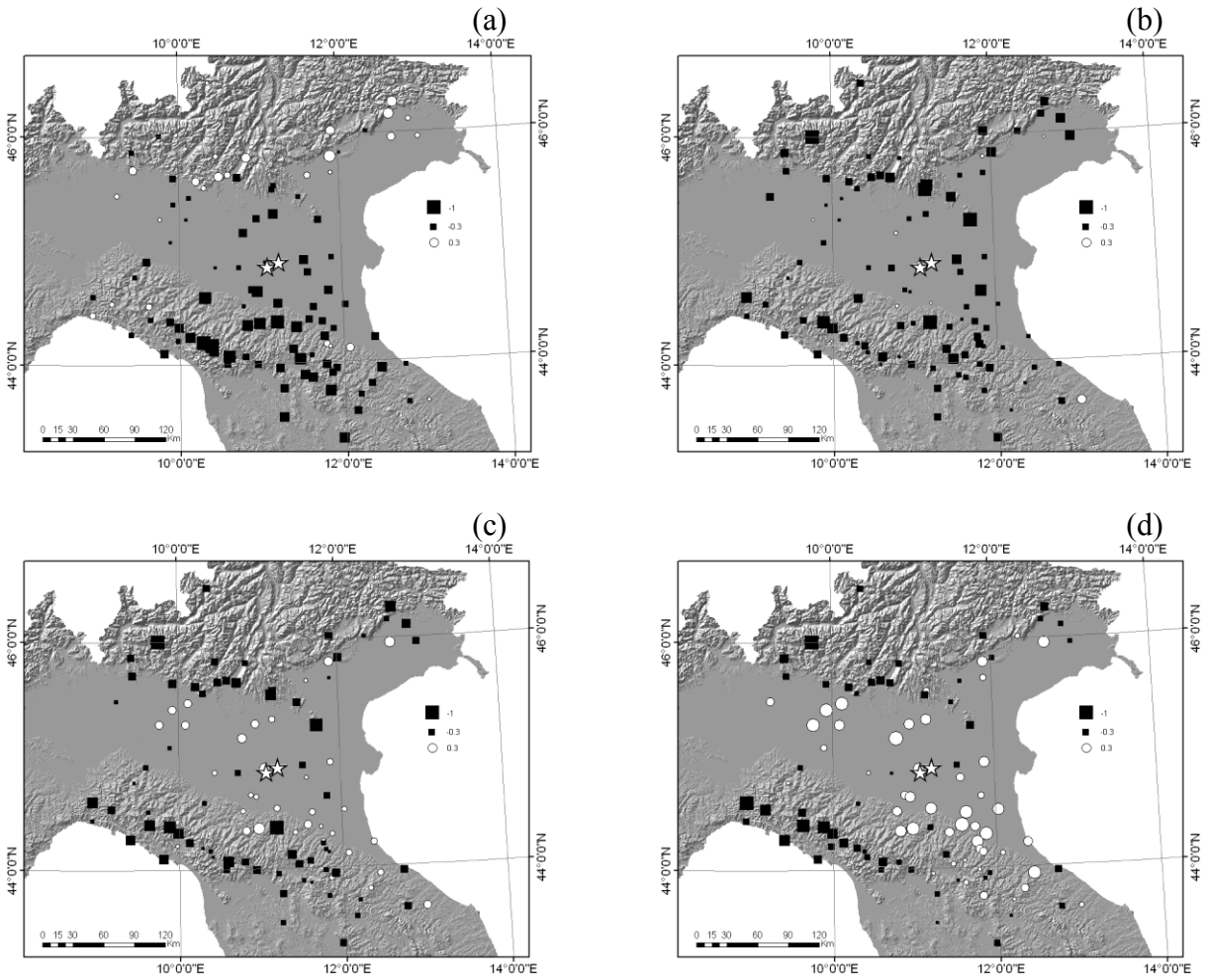

Figure 13.

Table 1.

Origin time * (UTC)	Latitude* (degrees)	Longitude* (degrees)	Depth* (Km)	Local magnitude*	Moment Magnitude**
2012/06/03 19:20:43	44.899	10.943	9.2	5.1	4.9
2012/05/29 11:00:25	44.879	10.947	5.4	5.2	
2012/05/29 10:55:57	44.888	11.008	6.8	5.3	5.5
2012/05/29 07:00:03	44.851	11.086	10.2	5.8	6.0
2012/05/20 13:18:02	44.831	11.49	4.7	5.1	5.2
2012/05/20 02:07:31	44.863	11.37	5	5.1	
2012/05/20 02:03:52	44.889	11.228	6.3	5.9	6.1

Table 2.

STA	LA_ST	LO_ST	EC8	# rec	Network
ALF	44.502	12.033	C*	2	IT
APR	46.156	10.158	C*	1	IT
ARG	44.630	11.825	D	2	IT
ARO	43.466	11.882	A*	1	IT
ASOL	45.800	11.902	A*	6	IV
AUL	44.208	9.973	A*	2	IT
BAG8	45.823	10.466	A*	6	IV
BBN	43.747	11.821	A	2	IT
BDG	44.507	9.623	A*	2	IT
BDI	44.062	10.597	A*	6	IV
BDT	43.706	12.188	A*	2	IT
BGL	43.995	10.576	A*	2	IT
BGN	44.322	9.992	B	2	IT
BOB	44.768	9.448	A*	3	IV
BON0	44.886	11.418	C**	1	IT
BORM	46.469	10.376	A*	5	IV
BOTT	45.549	10.310	A*	6	IV
BRA	46.004	9.762	C*	2	IT
BRB	43.954	11.212	A*	2	IT
BRH	44.208	11.764	B*	2	IT
BRIS	44.225	11.767	A*	3	IV
BRM	44.129	11.118	A*	1	IT
BRR	44.506	9.987	C*	1	IT
BSZ	44.031	11.467	A*	2	IT
CAFI	43.329	11.966	A*	4	IV
CAPR	45.637	9.935	B*	6	IV
CAS0	45.025	11.311	C**	1	IT
CES	44.210	12.386	B*	2	IT
CLA	46.271	12.514	B*	1	IT
CNCS	45.606	10.217	B	5	IV
CNF	44.110	10.411	A*	2	IT
CNG	45.882	12.288	B*	1	IT
CNT	44.723	11.287	C*	1	IT
COR1	43.632	13.000	B*	2	IV
CPC	44.921	11.876	C*	2	IT
CPGN	43.801	12.321	A	5	IV
CRND	45.836	12.013	C	6	IV
CRP	44.782	10.870	B*	1	IT
CSP	44.378	11.580	B*	2	IT
CST	45.660	11.902	B*	2	IT
CTL	43.955	12.735	C	2	IT
CTL8	45.276	9.762	C	6	IV
CTS	43.492	12.223	C*	1	IT
CVT	44.006	11.937	A*	1	IT

STA	LA_ST	LO_ST	EC8	# rec	Network
DCM	43.891	11.518	A	2	IT
EUCT	45.203	9.135	C*	1	IV
FAEN	44.290	11.877	C	2	IV
FDS	46.451	12.562	B*	1	IT
FER0	44.841	11.622	B*	1	IT
FGV	43.601	11.411	A*	1	IT
FIC0	44.521	11.434	C**	1	IT
FIE	43.807	11.294	A*	1	IT
FIN0	44.830	11.287	C**	1	IT
FIR	43.774	11.255	B	2	IV
FIVI	44.239	10.127	A*	1	GU
FLP	46.027	11.923	A*	2	IT
FRE1	44.118	11.382	C	2	IT
FRE8	46.015	12.355	A	5	IV
FRN	44.687	10.107	B*	1	IT
FVZ	44.238	10.131	E	2	IT
GAI	45.659	10.616	B*	2	IT
GNV	44.431	8.932	A	2	IT
IMOL	44.360	11.743	C	5	IV
ISD	45.273	10.960	B*	2	IT
LEC	45.861	9.412	B*	2	IT
LEOD	45.458	10.123	C	5	IV
LNG	44.655	10.313	C*	1	IT
LSP	44.096	9.807	A*	2	IT
MAJ	46.182	13.069	B*	1	IT
MBG0	44.719	11.534	C**	1	IT
MCR	43.800	12.448	C*	1	IT
MDC	44.486	11.640	C*	2	IT
MDG	44.159	11.789	A*	2	IT
MDN	44.646	10.889	C	2	IT
MDT	44.135	11.830	A*	2	IT
MERA	45.705	9.429	B*	6	IV
MILN	45.480	9.232	C*	6	IV
MLC	45.808	10.849	A*	2	IT
MLD	44.118	12.071	B*	2	IT
MMUR	43.442	12.997	A*	2	IV
MNS	45.252	11.722	C*	2	IT
MNTV	45.150	10.790	C*	6	IV
MODE	44.630	10.949	C*	6	IV
MOG0	44.932	10.912	C**	1	IT
MOMA	43.801	12.568	A*	1	IV
MOV	46.155	12.655	B*	2	IT
MPAG	43.629	12.760	A*	4	IV
MRN	44.878	11.062	C*	2	IT

STA	LA_ST	LO_ST	EC8	# rec	Network
MRR	44.064	11.603	A*	2	IT
MRZ	44.361	11.190	B*	2	IT
MTRZ	44.313	11.425	A*	4	IV
MURB	43.263	12.525	A*	2	IV
NEVI	44.581	10.313	A*	2	IV
NVL	44.843	10.732	C	2	IT
OPPE	45.308	11.172	C*	6	IV
ORZI	45.406	9.931	C*	6	IV
OSSC	43.524	11.246	A*	4	IV
OVD	44.636	8.642	C*	2	IT
PAR	44.828	10.279	B*	1	IT
PIT	43.989	10.944	A*	2	IT
PNM	44.379	9.881	C*	2	IT
PNN	43.818	12.263	A*	1	IT
POR	45.952	12.681	B*	2	IT
PRAD	46.248	12.889	B*	1	IT
PRM	43.979	11.781	A*	2	IT
PRT	44.149	10.926	A*	1	IT
PSR	45.949	13.014	B*	2	IT
PTV	45.274	10.088	B*	2	IT
PVF	44.333	10.825	A*	2	IT
PZS	44.188	10.288	E	2	IT
RAV0	44.716	11.143	C**	1	IT
RIM	44.005	12.485	C*	1	IT
RNC	43.870	11.607	A*	2	IT
RNS	44.595	8.936	B	2	IT
RVR	44.904	9.598	B*	2	IT
SAG0	44.791	11.390	C**	1	IT
SAN0	44.838	11.143	C**	1	IT
SANR	45.640	11.610	C	5	IV
SAS	44.483	8.486	C*	1	IT
SCEL	46.507	9.855	C*	1	CH
SEL	44.265	9.403	B	2	IT

STA	LA_ST	LO_ST	EC8	# rec	Network
SEM	46.485	10.271	C*	1	IT
SENI	43.705	13.233	B*	2	IV
SFI	43.905	11.850	A*	2	IV
SMP	44.064	10.803	A*	2	IT
SMS0	44.934	11.235	C**	1	IT
SNM	43.934	12.449	A*	2	IT
SNS	43.567	12.143	C	2	IT
SNZ1	45.074	9.894	C*	2	IT
SPI	46.108	12.905	B	2	IT
SRP	44.848	10.447	C*	2	IT
SSG	43.570	12.146	A*	1	IT
SSU	44.507	10.784	A*	2	IT
STAL	46.260	12.710	A*	3	IV
STS	43.942	11.905	C*	2	IT
STSP	46.627	10.333	C*	1	CH
T819	44.887	10.899	C**	1	IV
T820	44.791	11.573	C**	3	IV
T821	44.904	11.541	C**	3	IV
TGG	45.562	11.183	A*	2	IT
TGL	44.533	9.165	A*	2	IT
TREG	45.523	11.161	C*	6	IV
TVR	43.712	11.219	C*	1	IT
UMB	43.254	12.256	A*	2	IT
VGL	44.111	10.290	A*	1	IT
VLC	44.159	10.386	A*	2	MN
VLM	44.365	10.466	A*	1	IT
VOBA	45.643	10.504	B*	6	IV
VRL	44.392	9.633	B	2	IT
ZCCA	44.351	10.977	A*	5	IV
ZEN8	45.638	10.732	A*	5	IV
ZOVE	45.454	11.488	A*	6	IV
ZPP	44.524	11.204	C**	2	IT